Chapter 11
Fluctuation-Induced Forces Between Atoms and Surfaces: The Casimir–Polder Interaction

Francesco Intravaia, Carsten Henkel and Mauro Antezza

Abstract Electromagnetic fluctuation-induced forces between atoms and surfaces are generally known as Casimir–Polder interactions. The exact knowledge of these forces is rapidly becoming important in modern experimental set-ups and for technological applications. Recent theoretical and experimental investigations have shown that such an interaction is tunable in strength and sign, opening new perspectives to investigate aspects of quantum field theory and condensed-matter physics. In this chapter we review the theory of fluctuation-induced interactions between atoms and a surface, paying particular attention to the physical characterization of the system. We also survey some recent developments concerning the role of temperature, situations out of thermal equilibrium, and measurements involving ultra-cold atoms.

11.1 Introduction

In the last decade remarkable progress in trapping and manipulating atoms has opened a wide horizon to new and challenging experimental set-ups. Precision tests of both quantum mechanics and quantum electrodynamics have become

F. Intravaia (✉)
Theoretical Division, MS B213,
Los Alamos National Laboratory, Los Alamos, NM 87545, USA
e-mail: francesco_intravaia@lanl.gov

C. Henkel
Institut für Physik und Astronomie, Universität Potsdam, 14476, Potsdam, Germany
e-mail: carsten.henkel@physik.uni-potsdam.de

M. Antezza
Laboratoire Kastler Brossel, Ecole Normale Suprieure, CNRS and UPMC,
24 rue Lhomond, 75231, Paris, France
e-mail: mauro.antezza@lkb.ens.fr

possible through the capacity of addressing single trapped particles [1, 2] and of cooling ultracold gases down to Bose–Einstein condensation [3–5]. This stunning progress is also very profitable to other fundamental areas of physics and to technology. For example, ultracold gases have been suggested as probes in interesting experimental proposals aiming at very accurate tests of the gravity law [6–8], looking for extra forces predicted by different grand-unified theories [9] (see also the Chap. 3 by Milton in this volume for detailed discussions on the interplay between Casimir energy and gravity). Technologically speaking, one paradigmatic example of this new frontier is provided by atom chips [10, 11]. In these tiny devices, a cloud of atoms (typically alkalis like Sodium, Rubidium or Cesium) is magnetically or optically trapped above a patterned surface, reaching relatively short distances between a few microns to hundreds of microns [12–14]. The micro-machined surface patterns form a system of conducting wires, which are used to control the atomic cloud by shaping electromagnetic trapping fields (also super-conducting wires have been demonstrated [15–17]).

At a fundamental level, all these systems have in common to be strongly influenced by all kinds of atom–surface interactions. A particular category are fluctuation-induced forces, of which the most prominent representative is the van der Waals interaction [18]. These forces usually derive from a potential with a characteristic power-law dependence

$$\text{van der Waals limit:} \quad V = V_{\text{vdW}} \propto \frac{1}{L^n}, \tag{11.1}$$

where L is the distance between the objects (two atoms or a surface and a atom) and the exponent depends upon physical parameters and geometry of the system ($n = 3$ for an atom and a thick plate, see Fig. 11.1). Historically speaking, the existence of this kind of interaction was postulated long before it was experimentally possible to address single atoms [20]. The first quantum-mechanical theory was formulated by F. London in the 1930s using the idea that the quantum mechanical uncertainty of electrons in atoms can be translated into fluctuating electric dipole moments [21]. London found that two atoms attract each other following (11.1) with an exponent $n = 6$. London's theory was extensively applied in studying colloidal suspensions [22] which provided confirmations of its validity but also showed its limitations.

The next step was taken by H.B.G. Casimir and his student D. Polder [23] who applied the framework of quantum electrodynamics, including the concept of vacuum (field) fluctuations. They generalized the London–van der Waals formula by relaxing the electrostatic approximation, in other words, including the effect of retardation. The main success of Casimir–Polder theory was to provide an explanation for the change in the power law exponent observed in some experiments [22]. Indeed for distances larger than a characteristic length scale λ_0 of the system, the effect of retardation can no longer be neglected, and this leads to

$$\text{Casimir–Polder limit } L \gg \lambda_0: \quad V = V_{\text{CP}} \propto \frac{\lambda_0}{L^{n+1}}, \tag{11.2}$$
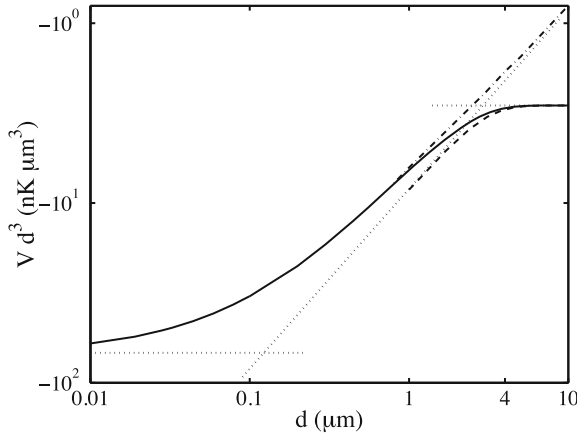
Fig. 11.1 Atom–surface potential [free energy of interaction $V(d)$] versus distance d between a
^{87}Rb atom and a SiO_2 (*sapphire*) substrate, multiplied by d^3. The potential is calculated using the
theory of Dzyaloshinskii, Lifshitz, and Pitaevskii (see see chapter VIII of [19]). Note the
logarithmic scale and the sign. The figure, adapted from Fig. 3 of [4], shows the potential at
$T = 300\,\mathrm{K}$ (*solid line*), at $T = 0\,\mathrm{K}$ (*dash-dotted line*), and the three asymptotic behaviors (*dotted
lines*): van der Waals–London $\propto -1/d^3$, Casimir–Polder ($\propto -1/d^4$), and Lifshitz ($\propto -T/d^3$)

and therefore to the L^{-7} dependence typical of the Casimir–Polder interaction
between two atoms. The scale λ_0 is in this case the wavelength of the main atomic
absorption lines, which is in the visible to near infrared for typical alkali atoms (of
the order of a few hundreds of nanometers).

The estimates (11.1, 11.2) apply at $T = 0$ when only quantum fluctuations play
a role. If the temperature is nonzero, another length scale comes into play, the
thermal or Wien wavelength

$$\lambda_T = \frac{\hbar c}{k_B T}, \tag{11.3}$$

which roughly corresponds to the wave length where the thermal radiation spec-
trum peaks. Calculations of the atom–surface interaction using thermal quantum
field theory have been pioneered by Dzyaloshinskii, Lifshitz, and Pitaevskii [19,
24]. They were able to recover the van der Waals and the Casimir–Polder
potentials as limit behavior of a more general expression and to confirm, quite
surprisingly, that at distances $L \ll \lambda_T$ the interactions are typically dominated by
quantum fluctuations, the main reason being that their spectrum is much wider
than that of the thermal field (which is constrained by the Bose–Einstein distri-
bution [25]). At distances $L \gg \lambda_T$ they show that the potential shows again a cross-
over from the Casimir–Polder to the Lifshitz asymptote:

$$\text{Lifshitz limit } L \gg \lambda_T: \quad V = V_\mathrm{L} \propto \frac{\lambda_0}{\lambda_T L^n} \sim \frac{k_B T}{\hbar \omega_0} V_\mathrm{vdW}, \tag{11.4}$$

where ω_0 is the (angular) frequency corresponding to λ_0. This potential that scales with temperature is actually a free energy of interaction and is also known as the Keesom potential between polar molecules: there, the dipoles are rotating freely under the influence of thermal fluctuations [26]. In this case (Rydberg atoms provide another example), the particle resonances overlap with the thermal spectrum, and the Casimir–Polder regime is actually absent. Equation (11.4) predicts an apparent enhancement, at nonzero temperature, of the fluctuation-induced interaction, relative to the Casimir-Polder limit.. This does not necessarily happen, however, because the molecular polarizabilities are also temperature-dependent [26–28].

In Fig.11.1 above, we considered the case of an alkali atom whose peak absorption wavelength λ_0 is much shorter than the Wien wavelength. The Lifshitz tail is then much smaller than the van der Waals potential. Note that λ_T is of the order of a few micrometers at room temperature, comparable to the smallest atom–surface distances achieved so far in atom chips. The crossover between the Casimir–Polder and the Lifshitz regimes can thus be explored in these set-ups. We discuss corresponding experiments in Sect. 11.5.

In the following sections, we start with a derivation of the interaction between an atom and a general electromagnetic environment (Sect. 11.2). We will refer to it using the term "atom–surface interaction" or "Casimir–Polder interaction". This term is also of common use in the literature to stress the fluctuation-induced nature of the interaction, although the term "Casimir–Polder" more correctly indicates the potential in the retarded limit (see (11.2)). The result will be valid within a second-order perturbation theory and can be easily adapted to specific geometries. We provide some details on a planar surface (Sect. 11.3). Situations out of global thermal equilibrium are discussed in Sect. 11.4, dealing with forces on ultracold atoms in a general radiation environment (the temperature of the surface and that of the surrounding environment are not necessarily the same), and with radiative friction. The final Sect. 11.5 sketches experiments with atomic beams and ultra-cold samples.

11.2 Understanding Atom–Surface Interactions

The interaction between atoms and surfaces plays a fundamental role in many fields of physics, chemistry and technology (see also the Chap. 12 of DeKieviet et al. in this volume for detailed discussions on modern experiments on atom–surface Casimir physics). From a quantum-mechanical point of view, fluctuation-induced forces are not surprising and almost a natural consequence of the initial assumptions. Indeed the existence of fluctuations, even at zero temperature, is one of the most remarkable predictions of the theory. Each observable corresponding to a physically measurable quantity can be zero on average but its variance will always be nonzero if the system is not in one of its eigenstates. When two quantum systems interact, the dynamics of the fluctuations becomes richer: each subsystem

Fig. 11.2 A schematic representation of the atom in the trap near a surface
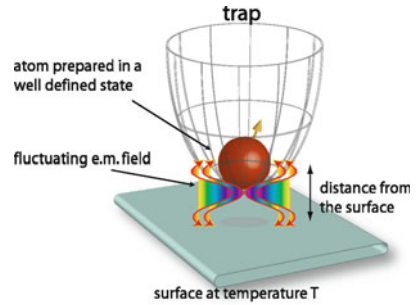
experiences, in addition to its own fluctuations, an external, fluctuating force. This becomes particularly clear in the case of a polarizable particle (atom or nanosphere) interacting with the vacuum electromagnetic field. In vacuum, the electromagnetic field fluctuates not only by itself, but also because there are fluctuating sources for it, like the electric dipole moment of the particle. At the same time, the particle's dipole is not only fluctuating on its own, but is also responding to the fluctuations of the electromagnetic field [29, 30]. As a result, when two atoms are brought nearby, they interact through their fluctuations mediated by the electromagnetic field. Similarly when a particle is in proximity of a macroscopic object, electric currents fluctuating inside the object and the fluctuations of the particle lead to a distance-dependent force. This second case is complicated by the fact of dealing with a macroscopic object and its quantum-mechanical description. However, if the medium responds linearly to an electromagnetic perturbation, the fluctuation-dissipation theorem [31] provides a connection between the field's autocorrelation function and its macroscopic response (or Green function) (Fig. 11.2).

We will use the previous considerations as a starting point for the derivation of the Casimir–Polder interaction between a surface and an atom or also a nanoparticle. We will follow Refs. [27, 32–34]. Although this is not the unique approach [23, 24, 35–42], it provides a physically transparent way to reach our final result.

11.2.1 Energy of a Polarizable Particle in an Electromagnetic Field

When a polarizable particle is introduced in an electric field, the change in energy of the system is given by [43]

$$\mathscr{F} = -\frac{\langle \mathbf{d}(t) \cdot \mathbf{E}(\mathbf{r}_0, t) \rangle}{2}, \tag{11.5}$$

where, since we are working in the Heisenberg representation, all the operators are time dependent. From the thermodynamic point of view the previous quantity is a

free energy and gives the amount of work that can be extracted from the system by moving the particle: in our (thermodynamic) convention a negative free energy will correspond to an attractive interaction (binding energy).

The expectation value $\langle \cdots \rangle$ is taken over the (initial) state of the non-coupled system; $\mathbf{d}$ is the (electric or magnetic) dipole operator and $\mathbf{E}$ the corresponding (electric or magnetic) field operator, evaluated at the dipole position $\mathbf{r}_0$. We are implicitly assuming that the size of the particle is small enough to locally probe the electromagnetic field (dipole approximation). The factor 1/2 in (11.5) arises from the fact that we are considering the energy of a linearly polarizable particle in an external field, rather than a permanent dipole [43]. Note that the choice of a particular ordering does not seem to be necessary at this stage since the dipole operator and the electric field operator commute. The symmetric order proves, however, to be particularly useful if we want to attach a physical meaning to each single contribution to the energy [29, 30], see (11.15).

The Hamiltonian of the coupled system can be in general written as $H = H_0 + V$, where H_0 is the sum of the Hamiltonians of the two isolated subsystems and V describes the interaction between them. Starting from this, the equation of motion for an operator $A(t)$ can be written in the following integral form (Heisenberg picture)

$$A(t) = A^{\text{free}}(t) + \frac{\mathrm{i}}{\hbar} \int\limits_0^t \mathrm{d}\tau \, e^{\frac{\mathrm{i}}{\hbar}H_0(t-\tau)}[V, A(\tau)] \, e^{\frac{\mathrm{i}}{\hbar}H_0(t-\tau)}, \qquad (11.6)$$

where $t = 0$ was chosen as initial time and the superscript free indicates that the operator evolves with respect to the Hamiltonian of the uncoupled system (H_0), i.e.

$$A^{\text{free}}(t) = e^{\frac{\mathrm{i}}{\hbar}H_0 t} A e^{-\frac{\mathrm{i}}{\hbar}H_0 t}. \qquad (11.7)$$

Now, within first-order perturbation theory, (11.6) can be solved by replacing the operator $A(\tau)$ under the integral by its corresponding free evolution. If the interaction Hamiltonian is bilinear like in the case of the electric dipole interaction, $V = -\mathbf{d} \cdot \mathbf{E}(\mathbf{r}_0)$, we get the following approximate expression for the dipole operator:

$$\mathbf{d}(t) \approx \mathbf{d}^{\text{free}}(t) + \mathbf{d}^{\text{ind}}(t), \qquad (11.8a)$$

$$\mathbf{d}^{\text{ind}}(t) = \int\limits_{-\infty}^{\infty} \mathrm{d}\tau \left(\frac{\mathrm{i}}{\hbar}[\mathbf{d}^{\text{free}}(t), \mathbf{d}^{\text{free}}(t-\tau)]\theta(\tau) \right) \cdot \mathbf{E}^{\text{free}}(\mathbf{r}_0, t-\tau), \qquad (11.8b)$$

and similarly for the field operator:

$$\mathbf{E}(\mathbf{r}, t) \approx \mathbf{E}^{\text{free}}(\mathbf{r}, t) + \mathbf{E}^{\text{ind}}(\mathbf{r}_0, t), \qquad (11.9a)$$

$$\mathbf{E}^{\text{ind}}(\mathbf{r}_0, t) = \int_{-\infty}^{\infty} \mathrm{d}\tau \left(\frac{\mathrm{i}}{\hbar}[\mathbf{E}^{\text{free}}(\mathbf{r}, t), \mathbf{E}^{\text{free}}(\mathbf{r}_0, t-\tau)]\theta(\tau) \right) \cdot \mathbf{d}^{\text{free}}(t-\tau). \qquad (11.9b)$$

The τ-integral runs effectively over $\tau \geq 0$ (note the step function $\theta(\tau)$) because in (11.6), only times $\tau > 0$ after the initial time are relevant (causality). In addition, we have set the upper limit to $\tau = \infty$ assuming that there exists a transient time τ_c after which the system behaviour becomes stationary. This time can be estimated from the system operators in (11.8b, 11.9b): the commutators are either c-number functions that die out for time arguments that differ by more than τ_c, or taking the expectation value, one gets subsystem correlation functions with τ_c as correlation time.

We have therefore that, within the first order perturbation theory, the dipole in addition to its unperturbed evolution ($\mathbf{d}^{\text{free}}(t)$) "responds" linearly ($\mathbf{d}^{\text{ind}}(t)$) to an external perturbation (in this case the electromagnetic field). The same also happens to the electromagnetic field where now the dipole is the external source of perturbation. The term in parenthesis under the integrals (11.8b, 11.9b), when evaluated over a particular state, is called *susceptibility* and contains the detailed physical information about the linear response of the system to the perturbation [29, 30]. In the particular case of a dipole the Fourier transform of the susceptibility tensor is the polarizability

$$\int_{-\infty}^{\infty} dt \frac{i}{\hbar} \langle a|[\mathbf{d}^{\text{free}}(t), \mathbf{d}^{\text{free}}(0)]|a\rangle \theta(t) e^{i\omega t} = \overleftrightarrow{\alpha}^a(\omega), \qquad (11.10)$$

where we have taken the expectation value for a given quantum state $|a\rangle$. In the time domain (see (11.8b)), the atomic susceptibility links the hermitean dipole operator to a hermitean field operator; hence it must be a real function. The polarizability, being its Fourier transform, therefore satisfies

$$[\overleftrightarrow{\alpha}^a(\omega)]^* = \overleftrightarrow{\alpha}^a(-\omega^*). \qquad (11.11)$$

In addition, because of causality, (11.10) implies that $\overleftrightarrow{\alpha}^a(\omega)$ must be analytical in the upper-half of the complex ω-plane.

Similar conclusions hold for the electromagnetic field. If we assume that the dynamics of the field and the surrounding matter (other than the atom) can be completely described in terms of bosonic operators [39, 44, 45], the result of the commutator in (11.9b) is a c-number and the susceptibility does not depend on the state of the radiation. The linearity of the Maxwell equations then ensures that the result of (11.9a,b) for a point-like dipole is correct to all orders. A simple identification leads to the following expression:

$$\int_{-\infty}^{\infty} \frac{i}{\hbar} [\mathbf{E}^{\text{free}}(\mathbf{r}, t), \mathbf{E}^{\text{free}}(\mathbf{r}_0, 0)] \theta(t) e^{i\omega t} dt = \overleftrightarrow{G}(\mathbf{r}, \mathbf{r}_0, \omega), \qquad (11.12)$$

where $\overleftrightarrow{G}$ is the electric field Green tensor, solution to the macroscopic Maxwell equation

$$-\nabla_{\mathbf{r}} \times \nabla_{\mathbf{r}} \times \overleftrightarrow{G}(\mathbf{r}, \mathbf{r}_0, \omega) + \frac{\omega^2}{c^2} \varepsilon(\mathbf{r}, \omega) \overleftrightarrow{G}(\mathbf{r}, \mathbf{r}_0, \omega) = -\frac{\omega^2}{\varepsilon_0 c^2} \delta(\mathbf{r} - \mathbf{r}_0) \overleftrightarrow{I}, \quad (11.13)$$

where $\overset{\leftrightarrow}{I}$ is the identity tensor and $\varepsilon(\mathbf{r}, \omega)$ is the local dielectric function (here supposed to be a scalar for simplicity) of the matter surrounding the dipole. In conclusion, in frequency space the induced quantities can be described in terms of the retarded response functions [43]

$$\mathbf{d}^{\mathrm{ind}}(\omega) = \overset{\leftrightarrow}{\alpha}(\omega) \cdot \mathbf{E}^{\mathrm{free}}(\mathbf{r}_0, \omega),$$
$$\mathbf{E}^{\mathrm{ind}}(\mathbf{r}, \omega) = \overset{\leftrightarrow}{G}(\mathbf{r}, \mathbf{r}_0, \omega) \cdot \mathbf{d}^{\mathrm{free}}(\omega), \tag{11.14}$$

where the frequency dependence and causality allow for a temporal delay. This is slightly schematic because the polarizability tensor is defined only when the average is taken.

Expressions (11.8a,b) and (11.9a,b) formalize the considerations made at the beginning of this section: both the dipole moment $\mathbf{d}(t)$ and the field $\mathbf{E}(t)$ can be split into two parts, the (free) fluctuating part describes the free intrinsic fluctuation, while the induced part arises in perturbation theory from the dipole coupling [25]. Equation (11.5) becomes

$$\mathscr{F} = -\frac{\langle \mathbf{d}^{\mathrm{ind}}(t); \mathbf{E}^{\mathrm{free}}(\mathbf{r}_0, t) \rangle}{2} - \frac{\langle \mathbf{E}^{\mathrm{ind}}(\mathbf{r}_0, t); \mathbf{d}^{\mathrm{free}}(t) \rangle}{2}. \tag{11.15}$$

We assumed a factorized initial state in which each free evolution operator is zero on average and where the correlations between the fluctuating parts are entirely encoded in the linear response functions, setting the correlation between the freely fluctuating components to zero. This assumption would break down at higher orders of perturbation theory. Note that while in (11.5) the total dipole and field operators (Heisenberg picture) commute at equal times, this is no longer true for their 'ind' and 'free' constituents in (11.15). The choice of the symmetric order (indicated by the semicolon) allows one to see each term of the previous expression as the result of the quantum expectation value of a Hermitian operator and therefore to attach to it a physical meaning [29, 30, 32]. The first term on the right hand side of (11.15) can be seen as the contribution to the Casimir–Polder energy coming from the fluctuations of the vacuum field; the second will be called the self-reaction term since it arises from the interaction of the dipole with the field generated by the dipole itself.

11.2.2 Equilibrium Fluctuations

Consider now a configuration at global thermal equilibrium, i.e. when both the dipole and the field are in a thermal state at temperature T. In this case we can apply the *fluctuation-dissipation theorem* [31]. This milestone of the linear response theory connects the correlation of a generic observable of a system in thermal equilibrium at temperature T with the imaginary part of the linear susceptibility which characterizes the response to a weak perturbation. In our case the theorem holds separately for the dipole and the field and we have [46–48]

$$\langle E_i^{\text{free}}(\mathbf{r}, \omega) E_j^{\text{free}}(\mathbf{r}, \omega') \rangle_T = 2\pi\hbar\delta(\omega + \omega') \coth\left(\frac{\hbar\omega}{2k_BT}\right) \text{Im}\left[G_{ij}(\mathbf{r}, \mathbf{r}, \omega)\right], \quad (11.16)$$

$$\langle d_i^{\text{free}}(\omega) d_j^{\text{free}}(\omega') \rangle_T = 2\pi\hbar\delta(\omega + \omega') \coth\left(\frac{\hbar\omega}{2k_BT}\right) \text{Im}\left[\alpha_{ij}^T(\omega)\right], \quad (11.17)$$

where the symbol $\langle \cdots \rangle_T$ define the quantum and the thermal average and, $\overset{\leftrightarrow}{\alpha}^T(\omega)$ defines the atomic polarizability operator evaluated at temperature T, according to (11.10) and (11.25).

$$\langle a^\dagger a + a a^\dagger \rangle_T = 1 + 2N(\omega) = \coth\left(\frac{\hbar\omega}{2k_BT}\right), \quad (11.18)$$

where $N(\omega)$ is the Bose–Einstein distribution. Note the asymptotic limits($\omega > 0$)

$$\coth\left(\frac{\hbar\omega}{2k_BT}\right) \rightarrow \begin{cases} 1 & T \ll \hbar\omega/k_B \\ \frac{2k_BT}{\hbar\omega} & T \gg \hbar\omega/k_B \end{cases} \quad (11.19)$$

in the "quantum" (low-temperature) and "classical" (high-temperature) limits.

The expression given in (11.16) can be directly reconnected with the currents fluctuating inside the media surrounding the dipole. For these currents Rytov's theory [49] predicts a correlation similar to (11.17) where the role of the polarizability is now played by the dielectric function [46–48] (see Sect. 11.4). This picture also lends itself to a natural generalization where the bodies are assumed to be in "local thermal equilibrium" (see Sect. 11.4.4).

Note that the field correlations are needed at the same position $\mathbf{r}_0$. The Green function is, however, divergent in this limit due to its free-space contribution

$$\overset{\leftrightarrow}{G}(\mathbf{r}, \mathbf{r}_0, \omega) = \underbrace{\overset{\leftrightarrow}{G_0}(\mathbf{r}, \mathbf{r}_0, \omega)}_{\text{freespace}} + \underbrace{\overset{\leftrightarrow}{\mathscr{G}}(\mathbf{r}, \mathbf{r}_0, \omega)}_{\text{scattered}}. \quad (11.20)$$

The corresponding part of the free energy provides the Lamb shift of the internal levels of the dipole immersed in the electromagnetic field [37]. This contribution is position-independent and does not contain any information about the interaction between the bodies and the dipole. Therefore it can be safely "hidden" in the (renormalized) energy levels of the atom. The physical information about the interaction is indeed contained only in the *scattered* part of the Green function [36]. If the body happens to be a plane surface, it follows from symmetry that the result can only depend on the dipole-surface distance L and we can set $\overset{\leftrightarrow}{\mathscr{G}}(\mathbf{r}_0; \mathbf{r}_0, \omega) \equiv \overset{\leftrightarrow}{\mathscr{G}}(L, \omega)$.

Combining (11.15–11.17), we finally obtain that the free energy of a polarizable particle at nonzero temperature T has the following general form (Einstein summation convention)

$$\mathscr{F}(L,T) = -\frac{\hbar}{2\pi} \int\limits_{0}^{\infty} d\omega \coth\left(\frac{\hbar\omega}{2k_BT}\right) \text{Im} \left[\alpha_{ij}^T(\omega)\mathscr{G}_{ji}(L,\omega)\right]. \qquad (11.21)$$

We have used the reality condition (11.11), implying that the imaginary part of both polarizability and Green tensors are odd in ω. Equation (11.21) coincides with the expression of the atom–surface interaction derived by many authors [23, 24, 27, 32–42]. It is often expressed in an equivalent form using the analyticity of $\overset{\leftrightarrow}{\alpha}^T(\omega)$ and $\overset{\leftrightarrow}{\mathscr{G}}(L,\omega)$ in the upper half of the complex frequency plane. Performing a (Wick) rotation to the imaginary frequency axis yields the so-called Matsubara expansion [24, 50]

$$\mathscr{F}(L,T) = -k_BT \sum_{n=0}^{\infty}{}'\alpha_{ij}^T(\mathrm{i}\xi_n)\mathscr{G}_{ji}(L,\mathrm{i}\xi_n), \qquad (11.22)$$

where the Matsubara frequencies $\xi_n = 2\pi n k_BT/\hbar$ arise from the poles of the hyperbolic cotangent, and the prime on the sum indicates that the $n = 0$ term comes with a coefficient 1/2. Both $\overset{\leftrightarrow}{\alpha}^T(\mathrm{i}\xi)$ and $\overset{\leftrightarrow}{\mathscr{G}}(L,\mathrm{i}\xi)$ are real expressions for $\xi > 0$ because of (11.10).

These considerations conclude our general analysis of the Casimir–Polder interaction. In the following section we will analyze the particle response function appearing in the previous formulation, namely the atomic polarizability, and mention also the case of a nanoparticle.

11.2.3 Polarizability Tensor

The previous results can be used for the interaction of a surface with atoms, molecules, particles or in general any (small) object that can be described with good approximation in terms of a electric-dipole polarizability tensor. Here we are going to review the polarizability of an atom and of a nanoparticle.

11.2.3.1 Atoms

The polarizability tensor is determined by the transition dipole matrix elements and the resonance frequencies. For an arbitrary atomic state $|a\rangle$ it can be written as

$$\alpha_{ij}^a(\omega) = \sum_b \frac{d_i^{ab}d_j^{ba}}{\hbar} \frac{2\omega_{ba}}{\omega_{ba}^2 - (\omega + \mathrm{i}0^+)^2}, \qquad (11.23)$$

where d_i^{ba} is the matrix element between the states $|b\rangle$ and $|a\rangle$ of the i-th component of the electric dipole operator and $\omega_{ba} = (E_b - E_a)/\hbar$ the corresponding

transition frequency. The introduction of an infinitesimal imaginary part shifts the poles of the expression into the lower part of the complex frequency plane $(\pm\omega_{ba} - i0^+)$, which is mathematically equivalent to the causality requirement. The tensorial form of the previous expression allows to take into account a possible anisotropic response of the atom to an electric field. A simplification can be obtained averaging over the different levels and directions so that the polarizability tensor becomes $\alpha_{ij}^a = \delta_{ij}\alpha_{\text{iso}}^a$ with the scalar function

$$\alpha_{\text{iso}}^a(\omega) = \sum_b \frac{|\mathbf{d}^{ba}|^2}{3\hbar} \frac{2\omega_{ba}}{\omega_{ba}^2 - (\omega + i0^+)^2}. \tag{11.24}$$

The polarizability is exactly isotropic when several excited sublevels that are degenerate in energy are summed over, like the $np_{x,y,z}$ orbitals of the hydrogen-like series. When the atom is in thermal equilibrium, we have to sum the polarizability over the states $|a\rangle$ with a Boltzmann weight:

$$\alpha_{ij}^T(\omega) = \sum_a \frac{e^{-E_a/k_BT}}{Z}\alpha_{ij}^a(\omega), \tag{11.25}$$

where Z is the partition function. In the limit $T \to 0$, we recover the polarizability for a ground state atom. For a single pair of levels $|a\rangle$ and $|b\rangle$, this leads to the following relation between the state-specific and the thermalized polarizabities:

$$\alpha_{ij}^T(\omega) \approx \alpha_{ij}^a(\omega) \tanh \frac{\hbar\omega_{ba}}{2k_BT}. \tag{11.26}$$

This is mainly meant to illustrate the temperature dependence, otherwise it is a quite crude approximation. The reason is that the coupling to other levels makes the polarizabilities α_{ij}^a and α_{ij}^b differ quite a lot. Electronically excited states are much more polarizable due to their larger electron orbitals.

11.2.3.2 Nanospheres

Let us consider now the case where the atom is replaced by a nanosphere [34, 51, 52]. When the sphere radius R is smaller than the penetration depth and the radiation wavelength, we can neglect higher order multipoles in the Mie expansion [53] and consider only the electric and magnetic dipole (the sphere is globally neutral).

In this long-wavelength limit, the Clausius–Mossotti relation [43, 54] provides the electric polarizability

$$\alpha_{\text{sph}}(\omega) = 4\pi\varepsilon_0 R^3 \frac{\varepsilon(\omega) - 1}{\varepsilon(\omega) + 2}, \tag{11.27}$$

where $\varepsilon(\omega)$ is the (scalar) dielectric function of the sphere's material. The nanosphere has also a magnetic polarizability that arises because a time-dependent

magnetic field induces circulating currents (Foucault currents) [43]. This leads to a diamagnetic response [55]

$$\beta_{\mathrm{sph}}(\omega) = \frac{2\pi}{15\mu_0}\left(\frac{R\omega}{c}\right)^2[\varepsilon(\omega) - 1]R^3. \qquad (11.28)$$

Both polarizabilities are isotropic (scalars). For a metallic sphere, the electric polarizability goes to a positive constant at zero frequency, while the magnetic one vanishes there and has a negative real part at low frequencies (diamagnetism).

For a qualitative comparison to an atom, one can estimate the oscillator strength [25], defined by the integral over the imaginary part of the polarizability. For the atom we have

$$\int\limits_0^\infty d\omega \,\mathrm{Im}\,\alpha_{\mathrm{at}}(\omega) \sim \frac{\pi(ea_0)^2}{\hbar} \quad\text{and}\quad \int\limits_0^\infty d\omega\,\mathrm{Im}\,\beta_{\mathrm{at}}(\omega) \sim \frac{\pi\mu_B^2}{\hbar}, \qquad (11.29)$$

where the Bohr radius a_0 and the Bohr magneton μ_B give the overall scaling of the transition dipole moments. The following dimensionless ratio allows a comparison between the two:

$$\frac{(ea_0)^2/\varepsilon_0}{\mu_B^2\mu_0} \sim \frac{1}{\alpha_{\mathrm{fs}}^2}, \qquad (11.30)$$

where $\alpha_{\mathrm{fs}} = e^2/(4\pi\varepsilon_0\hbar c) \approx 1/137$ is the fine structure constant. The electric oscillator strength clearly dominates in the atom.

Let us compare to a metallic nanosphere (gold is often used in experiments) and assume a Drude model (11.51) for the dielectric function. In terms of the volume $V = 4\pi R^3/3$, we get an electric oscillator strength

$$\int\limits_0^\infty \mathrm{Im}\,\alpha_{\mathrm{sph}}(\omega)d\omega = \frac{3}{2}\varepsilon_0\frac{\omega_p}{\sqrt{3}}V + \mathcal{O}\left(\frac{\gamma}{\omega_p}\right). \qquad (11.31)$$

where $\omega_p/\sqrt{3}$ is the resonance frequency of the particle plasmon mode (the pole of $\alpha_{\mathrm{sph}}(\omega)$, (11.27)). This is much larger than for an atom if the nanoparticle radius satisfies $a_0 \ll R \ll \lambda_p$, i.e., a few nanometers. The magnetic oscillator strength can be estimated as

$$\int\limits_0^{\omega_p} \mathrm{Im}\,\beta_{\mathrm{sph}}(\omega)d\omega = \frac{2\pi}{3\mu_0}\gamma\log\left(\frac{\omega_p}{\gamma}\right)\left(\frac{R}{\lambda_p}\right)^2 V. \qquad (11.32)$$

where we took ω_p as a cutoff frequency to make the integral convergent (at higher frequencies, (11.28) does not apply any more). We have used the plasma wavelength $\lambda_p = 2\pi c/\omega_p(\sim 100\,\mathrm{nm}$ for gold). Similar to an atom, the nanoparticle

response is dominantly electric, but the ratio of oscillator strengths can be tuned via the material parameters and the sphere size. The magnetic contribution to the particle–surface interaction is interesting because it features a quite different temperature dependence, see Ref. [27].

11.2.4 Non-perturbative Level Shift

In the previous section we saw that the main ingredient to derive the Casimir–Polder interaction between a particle and an object is the ability to solve for the dynamics of the joint system particle+electromagnetic field. Previously we limited ourself to a solution at the first order in the perturbation, implicitly motivated by the difficulty to solve *exactly* the dynamics of a multi-level atomic system coupled to a continuum of bosonic degrees of freedom (e.m. field). Things are different if we consider the linear coupling between two bosonic systems, i.e. if we describe the particle as a quantum harmonic oscillator. The linearity of the coupled system allows for an exact solution of its dynamics and even if the harmonic oscillator may be in some cases only a poor description of an atom [56], it is a good representation of a nanoparticle (the resonance frequency being the particle plasmon frequency). Generally, this approach gives a first qualitative indication for the physics of the interaction [57–61].

The main idea we follow in this section is based upon a generalization of the "remarkable formula" of Ford, Lewis and O'Connell [62, 63] (see also [57–61]). According to this formula, the free energy of a one-dimensional oscillator immersed in black body radiation is

$$\mathscr{F}_{\text{FLOC}}(T) = \frac{1}{\pi} \int_0^\infty d\omega \, f(\omega, T) \text{Im}[\partial_\omega \ln \alpha(\omega)], \tag{11.33}$$

where $f(\omega, T)$ is the free energy per mode,

$$f(\omega, T) = k_B T \log\left[2 \sinh\left(\frac{\hbar\omega}{2k_B T}\right)\right], \tag{11.34}$$

and $\alpha(\omega)$ is the (generalized) susceptibility of the oscillator derived from (11.39) below. More precisely, $\mathscr{F}_{\text{FLOC}}(T)$ gives the difference between two free energies: the oscillator coupled to the radiation field and in equilibrium with it, on the one hand, and solely the radiation field, on the other. Equation (11.33) is "remarkable" because the only system-relevant information needed here is the susceptibility function.

In three dimensions, the polarizability becomes a tensor

$$\mathbf{d}(\omega) = \overleftrightarrow{\alpha}(\omega) \cdot \mathbf{E}(\omega), \tag{11.35}$$

where $\mathbf{E}(\omega)$ is the external electric field. In the case considered by Ford, Lewis, and O'Connell, there was no need to include a spatial dependence because of the homogeneity and isotropy of the black body field. We are going to consider this symmetry to be broken by the presence of some scattering object. As a consequence, the generalized susceptibility tensor becomes position-dependent and anisotropic: $\overleftrightarrow{\alpha}(\omega, \mathbf{r}_0)$. The spatial dependence is connected with the scattered part of the Green function and leads both to a position-dependent frequency renormalization and a damping rate.

In order to get the expression of $\overleftrightarrow{\alpha}(\omega, \mathbf{r}_0)$, let us consider for simplicity the equation of motion of an isotropic oscillator with charge q interacting with the e.m. field near some scattering body (that is described by a dielectric constant). In frequency space, the (nonrelativistic) dynamics of the oscillator is described by

$$m\big[-\omega^2\mathbf{d}(\omega) + \omega_0^2\mathbf{d}(\omega)\big] = q^2\mathbf{E}(\mathbf{r}_0, \omega), \tag{11.36}$$

where we have neglected the coupling with the magnetic field (first order in $\dot{d}/c$). For the field we have

$$\nabla \times \nabla \times \mathbf{E}(\mathbf{r}, \omega) - \frac{\omega^2}{c^2}\varepsilon(\omega, \mathbf{r})\mathbf{E}(\mathbf{r}, \omega) = i\omega\mu_0\mathbf{j}(\mathbf{r}, \omega), \tag{11.37}$$

where the source current is $\mathbf{j}(\mathbf{r}, \omega) = -i\omega\mathbf{d}(\omega)\delta(\mathbf{r} - \mathbf{r}_0)$.

The formal exact solution for the operator $\mathbf{E}$ can be given in term of the (electric) Green tensor:

$$\mathbf{E}(\mathbf{r}, \omega) = \mathbf{E}^{\text{free}}(\mathbf{r}, \omega) + \overleftrightarrow{G}(\mathbf{r}, \mathbf{r}_0, \omega) \cdot \mathbf{d}(\omega), \tag{11.38}$$

where the Green tensor is the solution of (11.13) given above. The field $\mathbf{E}^{\text{free}}(\mathbf{r}, \omega)$ is the electromagnetic field we would have without the oscillator and it is connected with the intrinsic fluctuations of the polarization field, or equivalently, of the currents in the body. Physically (11.38) states that the total electromagnetic field is given by the field present near the scattering object plus the field generated by the dipole. Introducing (11.38) in (11.36) we get

$$-m(\omega^2 - \omega_0^2)\mathbf{d}(\omega) - q^2\overleftrightarrow{G}(\mathbf{r}_0; \mathbf{r}_0, \omega) \cdot \mathbf{d}(\omega) = q^2\mathbf{E}^{\text{free}}(\mathbf{r}_0, \omega). \tag{11.39}$$

The Green function $\overleftrightarrow{G}(\mathbf{r}; \mathbf{r}_0, \omega)$ solves Eq. (11.37) which describes an electromagnetic scattering problem and therefore, it decomposes naturally into a free-space field $\overleftrightarrow{G}_0$ (as if the source dipole were isolated in vacuum), and the field scattered by the body, $\overleftrightarrow{\mathscr{G}}$. This is at the basis of the splitting in (11.20) discussed above. The free-space part $\overleftrightarrow{G}_0(\mathbf{r}; \mathbf{r}_0, \omega)$ is a scalar in the coincidence limit because of the isotropy of space: schematically, part of the divergence $(\text{Re}[G_0])$ can be reabsorbed into mass renormalization, $m\omega_0^2 \mapsto m\tilde{\omega}_0^2$, and part $(\text{Im}[G_0])$ gives rise to dissipation (damping rate $\gamma(\omega)$[62,63]). Therefore (11.39) can be rewritten as

$$\left(-\omega^2 - \mathrm{i}\gamma(\omega)\omega + \tilde{\omega}_0^2 - \frac{q^2}{m}\overset{\leftrightarrow}{\mathscr{G}}(\mathbf{r}_0;\mathbf{r}_0,\omega)\right)\cdot\mathbf{d}(\omega) = \frac{q^2}{m}\mathbf{E}^{\mathrm{free}}(\mathbf{r}_0,\omega). \qquad (11.40)$$

The free electromagnetic field plays here the role of an external force and therefore the generalized (or "dressed") polarizability tensor is given by

$$\overset{\leftrightarrow}{\alpha}(\omega,\mathbf{r}_0) = \alpha_v(\omega)\left(1 - \alpha_v(\omega)\overset{\leftrightarrow}{\mathscr{G}}(\mathbf{r}_0;\mathbf{r}_0,\omega)\right)^{-1}, \qquad (11.41)$$

where we have defined

$$\alpha_v(\omega) = \frac{q^2}{m}\left(-\omega^2 - \mathrm{i}\gamma(\omega) + \tilde{\omega}_0^2\right)^{-1}. \qquad (11.42)$$

If Ford, Lewis and O'Connell's result is generalized to a three-dimensional oscillator, a trace operation appears before the logarithm in (11.33). Using the identity $\mathrm{tr}\log\overset{\leftrightarrow}{a} = \log\det\overset{\leftrightarrow}{a}$, one gets

$$\begin{aligned}
\mathscr{F}_{\mathrm{FLOC}}(T)\mathbf{r}_0 : \mathscr{F}_{\mathrm{FLOC}}(\mathbf{r}_0,T) &= \frac{1}{\pi}\int_0^\infty \mathrm{d}\omega\, f(\omega,T)\mathrm{Im}\left[\partial_\omega\ln\det\overset{\leftrightarrow}{\alpha}(\omega,\mathbf{r}_0)\right] \\
&= \frac{1}{\pi}\int_0^\infty \mathrm{d}\omega\, f(\omega,T)\mathrm{Im}[\partial_\omega\ln\alpha_v(\omega)] \\
&\quad - \frac{1}{\pi}\int_0^\infty \mathrm{d}\omega\, f(\omega,T)\mathrm{Im}\left[\partial_\omega\ln\det\left(1 - \alpha_v(\omega)\overset{\leftrightarrow}{\mathscr{G}}(\mathbf{r}_0;\mathbf{r}_0,\omega)\right)\right].
\end{aligned}$$
$$(11.43)$$

The first term is distance-independent and coincides with the free energy of an isolated oscillator in the electromagnetic vacuum. It can be interpreted as a free-space Lamb shift. The second part of (11.43) is distance-dependent and therefore gives rise to the Casimir–Polder interaction. In the case of a surface, with the help of a partial integration, we finally get

$$\mathscr{F}(L,T) = \frac{\hbar}{2\pi}\int_0^\infty \mathrm{d}\omega\coth\left(\frac{\hbar\omega}{2k_B T}\right)\mathrm{Im}\left[\ln\det\left(1 - \alpha_v(\omega)\overset{\leftrightarrow}{\mathscr{G}}(L,\omega)\right)\right]. \qquad (11.44)$$

The previous result can be easily generalized to the case of an anisotropic oscillator by just replacing the vacuum polarizability with the respective tensor.

The usual expression (11.21) for the Casimir Polder free energy is recovered by assuming a weak atom-field interaction. Expanding the logarithm to first order we get

$$\mathscr{F}(L,T) = -\frac{\hbar}{2\pi}\mathrm{Tr}\int_0^\infty \mathrm{d}\omega\coth\left(\frac{\hbar\omega}{2k_B T}\right)\mathrm{Im}\left[\alpha_v(\omega)\overset{\leftrightarrow}{\mathscr{G}}(L,\omega)\right]. \qquad (11.45)$$

From a scattering point of view, this approximation is equivalent to neglecting the multiple reflections of the electromagnetic field between oscillator and surface. At short distance to the surface, these reflections become relevant; the next-order correction to the van der Waals interaction arising from (11.44) is discussed in Sect. 12.3.4 of the chapter by DeKieviet et al. in this volume.

Note that although very similar, (11.21) and (11.45) are not identical. (11.21), applied to an oscillator atom, would have featured the bare polarizability

$$\alpha(\omega) = \frac{q^2/m}{\omega_0^2 - (\omega + i0^+)^2}, \qquad (11.46)$$

where the infinitesimal imaginary part $i0^+$ ensures causality. Equation (11.45) involves, on the contrary, the renormalized or vacuum-dressed polarizability which is causal by default. In other words, it contains a summation over an infinite subclass of terms in the perturbation series.

Finally, a general remark that connects with the scattering interpretation of dispersion forces (see Chap. 4 by Lambrecht et al. and Chap. 5 by Rahi et al. in this volume for detailed discussions on the calculation of the Casimir effect within the framework of the scattering theory): within the theory of two linearly coupled linear systems, the susceptibilities involved in the description of the equilibrium Casimir–Polder interaction are the *isolated and dressed* ones (isolated scatters). This means that, within a linear response theory, or equivalently up to the first order in the perturbation theory, the susceptibilities are not modified by the presence of the other scatters but only dressed by the electromagnetic field. In our case, this means that $\gamma(\omega)$ or $\tilde{\omega}$ in (11.44) or (11.45) do not depend on $\mathbf{r}_0$.

11.3 Atoms and a Planar Surface

Let us consider for definiteness the Casimir–Polder potential near a planar surface, with a distance L between the atom and surface. The Green function is in this case explicitly known and is given in the following subsection.

11.3.1 Behaviour of the Green function

In the case of a planar surface, the electromagnetic Green tensor can be calculated analytically, and we present here some of its main features. In our description we let the atom (source dipole) be on the positive z-axis at a distance L from the medium that occupies the half space below the xy-plane.

11.3.1.1 Reflection Coefficients and Material Response

The electric Green tensor $\overleftrightarrow{\mathcal{G}}(\mathbf{r}, \mathbf{r}_0, \omega)$ is needed for coincident positions $\mathbf{r} = \mathbf{r}_0$; by symmetry it is diagonal and invariant under rotations in the xy-plane [36, 46, 64, 65]:

$$
\overleftrightarrow{\mathcal{G}}(L, \omega)
$$
$$
= \frac{1}{8\pi\varepsilon_0} \int\limits_0^\infty kdk\,\kappa \left[\left(r^{\mathrm{TM}}(\omega, k) + \frac{\omega^2}{c^2\kappa^2} r^{\mathrm{TE}}(\omega, k) \right) [\hat{\mathbf{x}}\hat{\mathbf{x}} + \hat{\mathbf{y}}\hat{\mathbf{y}}] + 2\frac{k^2}{\kappa^2} r^{\mathrm{TM}}(\omega, k)\hat{\mathbf{z}}\hat{\mathbf{z}} \right] e^{-2\kappa L},
$$
$$(11.47)$$

where ε_0 is the vacuum permittivity, $k = |\mathbf{k}|$ is the modulus of the in-plane wave vector, and $\hat{\mathbf{x}}\hat{\mathbf{x}}$, $\hat{\mathbf{y}}\hat{\mathbf{y}}$, $\hat{\mathbf{z}}\hat{\mathbf{z}}$ are the cartesian dyadic products. We consider here a local and isotropic medium, excluding the regime of the anomalous skin effect [66]. The Fresnel formulae then give the following reflection coefficients in the TE- and TM-polarization (also known as s- and p-polarization) [43]:

$$
r^{\mathrm{TE}}(\omega, k) = \frac{\mu(\omega)\kappa - \kappa_m}{\mu(\omega)\kappa + \kappa_m}, \quad r^{\mathrm{TM}}(\omega, k) = \frac{\epsilon(\omega)\kappa - \kappa_m}{\epsilon(\omega)\kappa + \kappa_m}, \tag{11.48}
$$

where $\epsilon(\omega), \mu(\omega)$ are the permittivity and permeability of the medium. κ, κ_m are the propagation constants in vacuum and in the medium, respectively:

$$
\kappa = \sqrt{k^2 - \frac{\omega^2}{c^2}}, \quad \kappa_m = \sqrt{k^2 - \varepsilon(\omega)\mu(\omega)\frac{\omega^2}{c^2}}. \tag{11.49}
$$

The square roots are defined so that $\operatorname{Im}\kappa, \operatorname{Im}\kappa_m \leq 0$ and $\operatorname{Re}\kappa, \operatorname{Re}\kappa_m \geq 0$. In particular κ is either real or pure imaginary. The corresponding frequencies and wave vectors define two regions in the (ω, k) plane [54]: *Evanescent region* $\omega < ck$: the electromagnetic field propagates only parallel to the interface and decays exponentially ($\kappa > 0$) in the orthogonal direction. *Propagating region* $\omega > ck$: the electromagnetic field also propagates ($\operatorname{Re}\kappa = 0$) in the orthogonal direction. Note that the magnetic Green tensor $\overleftrightarrow{\mathcal{H}}$ can be obtained from the electric one by swapping the reflection coefficients [67]:

$$
\varepsilon_0 \overleftrightarrow{\mathcal{G}} \equiv \frac{1}{\mu_0} \overleftrightarrow{\mathcal{H}} (r^{\mathrm{TE}} \leftrightarrow r^{\mathrm{TM}}). \tag{11.50}
$$

All information about the optical properties of the surface is encoded in the response functions $\varepsilon(\omega)$ and $\mu(\omega)$. For the sake of simplicity, we focus in the following on a nonmagnetic, metallic medium ($\mu(\omega) = 1$) and use the Drude model [43]:

$$
\varepsilon(\omega) = 1 - \frac{\omega_p^2}{\omega(\omega + i\gamma)}, \tag{11.51}
$$

where ω_p is the plasma frequency (usually for metals in the UV regime). The dissipation rate γ takes account of all dissipative phenomena (impurities, electron-phonon scattering, etc.) in the metal [68] and generally $\gamma/\omega_p \ll 1$ ($\sim 10^{-3}$ for gold).

11.3.1.2 Distance Dependence of the Green Tensor

The Drude model includes Ohmic dissipation in a very characteristic way, through the parameter γ. This affects the physical length scales of the system (see Ref. [69] for a review). In our case the relevant ones are the photon wavelength in vacuum λ_ω and the skin depth in the medium δ_ω. While the first is simply given by

$$\lambda_\omega = \frac{2\pi c}{\omega},\tag{11.52}$$

the second is defined in terms of the low frequency behavior of the dielectric function

$$\frac{1}{\delta_\omega} = \frac{\omega}{c}\mathrm{Im}\sqrt{\varepsilon(\omega)} \approx \sqrt{\frac{\omega}{2D}} \quad (\text{for } \omega \ll \gamma),\tag{11.53}$$

where $D = \gamma c^2/\omega_p^2$ is the diffusion coefficient for the magnetic field in a medium with Ohmic damping [43]. The skin depth gives a measure of the penetration of the electromagnetic field in the medium ($\sim 0.79\,\mu\mathrm{m}$ at 10 GHz for gold). If we have $\delta_\omega \ll \lambda_\omega$, the dependence of the Green function on L is quite different in the following three domains: (i) the *sub-skin-depth region*, $L \ll \delta_\omega$, (ii) the *non-retarded region*, $\delta_\omega \ll L \ll \lambda_\omega$, (iii) the *retarded region*: $\lambda_\omega \ll L$. In zones (i) and (ii), retardation can be neglected (van-der-Waals zone), while in zone (iii), it leads to a different power law (Casimir–Polder zone) for the atom–surface interaction.

In the three regimes, different approximations for the reflection coefficients that appear in (11.47) can be made. In the *sub-skin-depth zone* [67], we have $k \gg 1/\delta_\omega \gg 1/\lambda_\omega$ and

$$\begin{aligned} r^{\mathrm{TE}}(\omega,k) &\approx [\varepsilon(\omega) - 1]\frac{\omega^2}{4c^2k^2}, \\ r^{\mathrm{TM}}(\omega,k) &\approx \frac{\varepsilon(\omega) - 1}{\varepsilon(\omega) + 1}\left[1 + \frac{\varepsilon(\omega)}{\varepsilon(\omega) + 1}\frac{\omega^2}{c^2k^2}\right]. \end{aligned}\tag{11.54}$$

At intermediate distances in the *non-retarded zone*, the wave vector is $1/\lambda_\omega \ll k \ll 1/\delta_\omega$, hence

$$\begin{aligned} r^{\mathrm{TE}}(\omega,k) &\approx -1 + \mathrm{i}\frac{2}{\sqrt{\varepsilon(\omega)}}\frac{ck}{\omega}, \\ r^{\mathrm{TM}}(\omega,k) &\approx 1 + \mathrm{i}\frac{2}{\sqrt{\varepsilon(\omega)}}\frac{\omega}{ck}. \end{aligned}\tag{11.55}$$

Table 11.1 Magnetic and electric Green tensors at a planar surface

	Sub-skin depth	Non-retarded	Retarded
$\mathscr{G}_{xx}$	$\frac{1}{32\pi\varepsilon_0 L^3}\left(1-\frac{2}{\varepsilon(\omega)}\right)$		$\frac{1}{32\pi\varepsilon_0 L^3}\left(1-\frac{2}{\varepsilon(\omega)}\right)\left(1-\mathrm{i}\frac{4\pi L}{\lambda_\omega}-\frac{1}{2}\left[\frac{4\pi L}{\lambda_\omega}\right]^2\right)e^{4\pi\mathrm{i}L/\lambda_\omega}$
$\mathscr{H}_{xx}$	$\frac{\mathrm{i}\mu_0}{32\pi\delta_\omega^2 L}$	$-\frac{\mu_0}{32\pi L^3}$	$-\frac{\mu_0}{32\pi L^3}\left(1-\mathrm{i}\frac{4\pi L}{\lambda_\omega}-\frac{1}{2}\left[\frac{4\pi L}{\lambda_\omega}\right]^2\right)e^{4\pi\mathrm{i}L/\lambda_\omega}$

In this case the other elements have the asymptotes $\mathscr{H}_{yy}=\mathscr{H}_{xx}$, $\mathscr{H}_{zz}=2\mathscr{H}_{xx}$, and similarly for $\mathscr{G}_{ii}$. The off-diagonal elements vanish. The expressions are for metals where $|\varepsilon(\omega)|\gg 1$.

Finally, in the *retarded zone* we can consider $k\ll 1/\lambda_\omega\ll 1/\delta_\omega$, so that

$$r^{\mathrm{TE}}(\omega,k)\approx -1+\frac{2}{\sqrt{\varepsilon(\omega)}},$$
$$r^{\mathrm{TM}}(\omega,k)\approx 1-\frac{2}{\sqrt{\varepsilon(\omega)}}. \tag{11.56}$$

Note that the first terms in (11.55, 11.56) correspond to a perfectly reflecting medium (formally, $\varepsilon\to\infty$).

The asymptotics of the Green tensor that correlate to these distance regimes are obtained by performing the k-integration in (11.47) with the above approximations for the reflection coefficients. The leading-order results are collected in Table 11.1. One notes that the zz-component is larger by a factor 2 compared to the xx-and yy-components. This difference between the normal and parallel dipoles can be understood by the method of images [43].

The magnetic response for a normally conducting metal in the sub-skin-depth regime is purely imaginary and scales linearly with the frequency ω: the reflected magnetic field is generated by induction. A significant response to low-frequency magnetic fields appears for superconductors because of the Meissner–Ochsenfeld effect [70]. In contrast, the electric response is strong for all conductors because surface charges screen the electric field efficiently.

The imaginary part of the trace of the Green tensor determines the local mode density (per frequency) for the electric or magnetic fields [71]. These can be compared directly after multiplying by ε_0 (or $1/\mu_0$), respectively. As is discussed in Refs. [69, 71], in the sub-skin-depth regime near a metallic surface, the field fluctuations are mainly of magnetic nature. This can be traced back to the efficient screening by surface charges connected with electric fields. Magnetic fields, however, cross the surface much more easily as surface currents are absent (except for superconductors). This reveals, to the vacuum outside the metal, the thermally excited currents within the bulk.

11.3.2 Asymptotic Power Laws

To begin with, let us assume that the particle and the field are both at zero temperature. The Matsubara series in (11.22) can be replaced by an integral over imaginary frequencies:

$$\mathscr{F}(L) = -\frac{\hbar}{2\pi} \int\limits_0^\infty \mathrm{d}\xi \sum_j \alpha_{jj}^g(\mathrm{i}\xi) \mathscr{G}_{jj}(L, \mathrm{i}\xi), \tag{11.57}$$

where we have used the fact that the Green tensor is diagonal. Alternatively one can get the previous result by taking the limit $T \to 0$ of (11.21) and performing a Wick rotation on the imaginary axis. One of the main advantages of this representation is that all functions in (11.57) are real. For electric dipole coupling, one has $\alpha_{ii}^g(\mathrm{i}\xi), \mathscr{G}_{ii}(L, \mathrm{i}\xi) > 0$, and we can conclude that the (11.57) is a binding energy and corresponds to an attractive force (see the Chap. 8 by Capasso et al. in this volume for detailed discussion on repulsive fluctuation-induced forces in liquids).

Along the imaginary axis, the Green tensor is dominated by an exponential $\mathrm{e}^{-2\xi L/c}$, see (11.47). This exponential suppresses large values of ξ and the main contribution to the integral comes from the region $\xi < c/(2L)$. If this value is smaller than the characteristic frequency, say Ω_e, of the atom or of the nanoparticle (the lowest transition in (11.23)), the polarizability can be approximated by its static value. Assuming an isotropic polarizability we get the Casimir–Polder asymptote ($\lambda_e = c/(2\Omega_e)$)

$$L \gg \lambda_e: \quad \mathscr{F}(L)_{\mathrm{CP}} \approx -\frac{3\hbar c \alpha_{\mathrm{iso}}^g(0)}{2^5 \pi^2 \varepsilon_0 L^4}, \tag{11.58}$$

which is the well known expression for the atom–surface Casimir–Polder interaction [23]. At short distance the polarizability limits the relevant frequency range to $\xi \lesssim \Omega_e$. Therefore for $L \ll \lambda_e$ we can replace Green tensor by its short distance approximation (see Table 11.1) where it becomes independent of ξ. We recover then the van der Waals asymptote

$$L \ll \lambda_e: \quad \mathscr{F}(L)_{\mathrm{vdW}} \approx -\frac{\hbar}{2^4 \pi^2 \varepsilon_0 L^3} \int\limits_0^\infty \mathrm{d}\xi \alpha_{\mathrm{iso}}^g(\mathrm{i}\xi). \tag{11.59}$$

Similar expressions hold for the interaction due to a fluctuating magnetic dipole, the behaviour becoming more complicated when the distance becomes comparable to a characteristic skin depth (see (11.53) and Ref. [27]).

If we write the Matsubara frequencies as $\xi_n = 2\pi n c/\lambda_T$ ($n = 0, 1, 2, \ldots$), the temperature may be low enough so that the limit $\lambda_T \gg L$ holds. Then all Matsubara frequencies are relevant, and if they are dense enough ($\lambda_T \gg \lambda_e$), the effect of temperature is negligible. The series in (11.22) is then well approximated by the integral in (11.57). In the opposite (high-temperature) limit, one has $\lambda_T \ll L$ so that the exponential behavior of the Green tensor limits the series in (11.22) to its first term recovering the Lifshitz asymptote

$$\mathscr{F}(L, T) \approx -\frac{k_B T \alpha_{\mathrm{iso}}^g(0)}{16\pi \varepsilon_0 L^3}. \tag{11.60}$$

We still have an attractive force. Note, however, that this attraction is mainly due to the classical part of the radiation, as the same result would be obtained with a polarizable object immersed into the thermal field.

11.4 Beyond Equilibrium

11.4.1 Overview

The theory presented so far has mainly considered the atom, the field, and the surface to be in a state of global thermal equilibrium, characterized by the same temperature T. When one moves away from these conditions, the atom–surface interaction assumes novel features like metastable or unstable states, driven steady states with a nonzero energy flux etc. We review some of these aspects here, since they have also appeared in recent experiments (Sect. 11.5). On the theoretical side, there are a few controversial issues that are currently under investigation [72–74].

We start with atoms prepared in non-thermal states: ground or excited states that decay by emission or absorption of photons, and with atoms in motion where frictional forces appear. We then consider field–surface configurations out of global equilibrium like a surface surrounded by a vacuum chamber at different temperature.

11.4.2 Atoms in a Given State and Field in Thermal Equilibrium

The generalization of the Casimir–Polder potential to an atom in a definite state $|a\rangle$ can be found, for example, in Wylie and Sipe [36], (4.3, 4.4). The fluctuation–dissipation theorem for the dipole, (11.17), does not apply, but perturbation theory is still possible, with the result (summation over repeated indices i, j)

$$\mathscr{F}(L,T) = -k_B T \sum_{n=0}^{\infty}{}' \alpha_{ij}^a(\mathrm{i}\xi_n)\mathscr{G}_{ji}(L,\mathrm{i}\xi_n) + \sum_b N(\omega_{ba})d_i^{ab}d_j^{ba}\mathrm{Re}[\mathscr{G}_{ji}(L,\omega_{ba})],$$

(11.61)

where $\overset{\leftrightarrow}{\alpha}^a$ is the state-dependent polarizability [36, 75]. The dipole matrix elements are written $d_i^{ab} = \langle a|d_i|b\rangle$. The thermal occupation of photon modes (Bose–Einstein distribution) is

$$N(\omega) = \frac{1}{e^{\hbar\omega/k_B T} - 1} = -1 - N(-\omega).$$

(11.62)

Note the second term in (11.61) that is absent in thermal equilibrium. It involves the absorption and (stimulated) emission of photons on transitions $a \to b$ to other

quantum states, and the thermal occupation number $N(\omega_{ba})$ evaluated at the Bohr frequency $\hbar\omega_{ba} = E_b - E_a$. For this reason, it can be called *resonant* part. The first term that was also present in equilibrium now features the state-dependent polarizability tensor $\overset{\leftrightarrow}{\alpha}^a(i\xi_n)$. This is the *non-resonant* part of the interaction.

For the alkali atoms in their ground state $|a\rangle = |g\rangle$, the Bohr frequencies E_{bg} are all positive (visible and near-infrared range) and much larger than typical laboratory temperatures (equivalent to the THz range), hence the thermal occupation numbers $N(\omega_{ba})$ are negligibly small. By the same token, the ground-state polarizability is essentially the same as in thermal equilibrium $\overset{\leftrightarrow}{\alpha}^T(i\xi_n)$ because the thermal occupation of the excited states would come with an exponentially small Boltzmann weight. The atom–surface interaction is then indistinguishable from its global equilibrium form and dominated by the non-resonant part.

With suitable laser fields, one can perform the spectroscopy of atom–surface interaction of excited states $|a\rangle = |e\rangle$. It is also possible to prepare excited states by shining a resonant laser pulse on the atom. In front of a surface, the second term in (11.61) then plays a dominant role: the transition to the ground state where a real photon is emitted is accompanied by an energy shift proportional to $\text{Re}[\overset{\leftrightarrow}{\mathscr{G}}(L, -\omega_{eg})]$. This resonant contribution can be understood in terms of the radiation reaction of a classical dipole oscillator [36, 76]: one would get the same result by asking for the frequency shift of an oscillating electric dipole in front of a surface—a simple interpretation in terms of an image dipole is possible at short distances (where the k-dependence of the reflection coefficients (11.48) can be neglected). This term is essentially independent of temperature if the transition energy E_{eg} is above $k_B T$.

A more familiar effect for the excited state is spontaneous decay, an example for a non-stationary situation one may encounter out of thermal equilibrium. We can interpret the resonant atom–surface interaction as the 'reactive counterpart' to this dissipative process. Indeed, the spontaneous decay rate is modified relative to its value in free space by the presence of the surface. This can also be calculated in classical terms, leading to a modification that involves the imaginary part of the Green tensor $\overset{\leftrightarrow}{G}(L, \omega_{eg})$. (The free-space contribution $\overset{\leftrightarrow}{G}_0$ has a finite imaginary part.) In fact, both the decay rate and the interaction potential can be calculated from a complex quantity, formally equivalent to an "effective self-energy", of which (11.61) is the real part in the lowest non-vanishing order of perturbation theory.

What happens if the Bohr frequencies $\hbar\omega_{ba}$ become comparable to $k_B T$? This applies, for example, to optically active vibrational transitions and to atoms in highly excited states (Rydberg atoms) where the energy levels are closely spaced. It is obvious from (11.61) that the resonant term is subject to cancellations among "up" ($E_b > E_a$) and "down" transitions ($E_{b'} < E_a$) with nearly degenerate Bohr frequencies: the occupation numbers $N(\omega_{ba})$ and $N(\omega_{b'a})$ differ in sign, while $\text{Re}[\overset{\leftrightarrow}{\mathscr{G}}(L, \omega)]$ is even in ω. To leading order in the high-temperature limit, the resonant term becomes

$$\mathscr{F}^{\text{res}}(L, T) \approx \frac{k_B T}{\hbar} \left[\sum_{b > a} \frac{\text{Re}\mathscr{G}^{ba}(L, \omega_{ba})}{\omega_{ba}} - \sum_{b' < a} \frac{\text{Re}\mathscr{G}^{b'a}(L, \omega_{ab'})}{\omega_{ab'}} \right], \qquad (11.63)$$

$$\mathscr{G}^{ba}(L, \omega) = d_i^{ab} d_j^{ba} \mathscr{G}_{ij}(L, \omega), \qquad (11.64)$$

where the notation $b > a$ and $b < a$ means summing over states with energies E_b above or below E_a. This is proportional to the anharmonicity of the atomic level spectrum around E_a. It vanishes exactly for a harmonic oscillator and reduces significantly the coefficient linear in temperature in weakly anharmonic regions of the atomic spectrum [28].

11.4.3 Moving Atoms

An atom that moves in a radiation field can be subject to a frictional force, as pointed out by Einstein in his seminal 1917 paper on the blackbody spectrum [77]. This force originates from the aberration and the Doppler shift between the field the atom "sees" in its co-moving frame, and the "laboratory frame". (The latter frame is actually defined in terms of the thermal distribution function of the radiation field that is not Lorentz-invariant. Only the field's vacuum state in free space is Lorentz-invariant.) In addition, electric and magnetic fields mix under a Lorentz transformation so that a moving electric dipole also carries a magnetic moment proportional to $\mathbf{d} \times \mathbf{v}$ where $\mathbf{v}$ is the (center-of-mass) velocity of the dipole (the Röntgen current discussed in Refs. [78–81]).

11.4.3.1 Black Body Friction

The free-space friction force $\mathbf{f}(\mathbf{v}, T)$ is given by [82, 83]:

$$\mathbf{f}(\mathbf{v}, T) = -\mathbf{v} \frac{\hbar^2 / k_B T}{12\pi^2 \varepsilon_0 c^5} \int_0^\infty d\omega \frac{\omega^5 \text{Im}\,\alpha(\omega)}{\sinh^2(\hbar\omega / 2k_B T)}, \qquad (11.65)$$

where $\alpha(\omega)$ is the polarizability of the atom (in its electronic ground state) and the approximation of slow motion (first order in $\mathbf{v}/c$) has been made. For atomic transitions in the visible range, this force is exponentially suppressed by the Boltzmann factor $\sim e^{-\hbar\omega_{eg}/k_B T}$ that is winning against the prefactor $1/T$ in (11.65). The physics behind this effect is the same as in Doppler cooling in two counter-propagating laser beams: the friction arises from the frequency shift in the frame co-moving with the atom that breaks the efficiency of absorbing photons with counter- and co-propagating momenta. Einstein derived the Maxwell–Boltzmann distribution for the atomic velocities by balancing this radiative friction with the momentum recoil in randomly distributed directions as the absorbed photons are

re-emitted, which leads to Brownian motion in velocity space [77, 84]. Conversely, assuming thermal equilibrium and the validity of the Einstein relation between momentum diffusion and friction, one can calculate the (linear) friction tensor $\overleftrightarrow{\Gamma}$ in $\mathbf{f}(\mathbf{v}) = -\overleftrightarrow{\Gamma}\mathbf{v}$ from the correlation function of the force operator [83, 85]:

$$\overleftrightarrow{\Gamma} = \frac{1}{k_B T} \int\limits_{-\infty}^{+\infty} d\tau \langle \mathbf{F}(t + \tau); \mathbf{F}(t) \rangle, \tag{11.66}$$

where $\mathbf{F}(t)$ is the force operator in the Heisenberg picture, the operator product is symmetrized (as in Sect. 11.2.1), and the average $\langle \cdots \rangle$ is taken at (global) thermal equilibrium. One recognizes in (11.66) the zero-frequency component of the force correlation spectrum.

The motion of atoms in the radiation field plays a key role for laser cooling of ultracold gases. Although a discussion of laser-induced forces is beyond the scope of this chapter, the basic principles can be illustrated by moving away from global equilibrium and assigning temperatures T_A, T_F to atom and field. An ultracold gas, immediately after switching off the lasers, would correspond to T_A in the nano-Kelvin range, while $T_F = 300$ K is a good assumption for the fields in a non-cryogenic laboratory apparatus. Dedkov and Kyasov calculated the separate contributions from fluctuations of the atomic dipole and the field, respectively. We follow here Ref. [86]. Qualitatively speaking, the fluctuating dipole experiences a force when it emits a photon; this force is nonzero and depends on velocity, even after averaging over all emission directions, because the emission is isotropic only in the rest frame of the atom. The absorption of photons from the fluctuating field is accompanied by photon recoil, and here isotropy is broken because the Doppler shift brings certain directions closer to the resonance frequency. The same principle is behind the so-called Doppler cooling in two counterpropagating beams. The sum of the two contributions takes the form (adapted from (29) of Ref. [86])

$$\hat{\mathbf{v}} \cdot \mathbf{f}(\mathbf{v}) = -\frac{\hbar}{4\pi\varepsilon_0 c \gamma_{\mathbf{v}}} \int \frac{d^3 k}{\pi^2} (\hat{\mathbf{k}} \cdot \hat{\mathbf{v}})(\omega')^2 \text{Im}\,\alpha(\omega')(N(\omega, T_F) - N(\omega', T_A)) \tag{11.67}$$

$$\omega' = \gamma_{\mathbf{v}}(\omega + \mathbf{k} \cdot \mathbf{v}), \tag{11.68}$$

where $\gamma_{\mathbf{v}} = (1 - \mathbf{v}^2/c^2)^{-1/2}$ is the relativistic Lorentz factor, and $\hat{\mathbf{v}}$, $\hat{\mathbf{k}}$ are unit vectors along the atom's velocity and the photon momentum. The photon frequency in the "blackbody frame" (field temperature T_F) is $\omega = c|\mathbf{k}|$, and $N(\omega, T)$ is the Bose–Einstein distribution for a mode of energy quantum $\hbar\omega$ at temperature T. The term with $N(\omega, T_F)$ gives the force due to absorption of thermal photons, while $N(\omega', T_A)$ gives the force due to dipole fluctuations. The absorbed power has to be calculated in the atom's rest frame: the energy $\hbar\omega'$ times the photon number provides the electric field energy density in this frame, and the absorption spectrum $\text{Im}[\omega'\alpha(\omega')]$ must be evaluated at the Doppler-shifted frequency ω'. This

shifted spectrum also appears in the fluctuation-dissipation theorem (11.17) now applied locally in the atom's rest frame, and determines the dipole fluctuations.

At equilibrium and in the non-relativistic limit, the difference between the Bose–Einstein distributions can be expanded to give

$$N(\omega, T_F) - N(\omega', T_A) \approx -(\mathbf{k} \cdot \mathbf{v}) \partial_\omega N(\omega, T) = (\mathbf{k} \cdot \mathbf{v}) \frac{\hbar/k_B T}{4 \sinh^2(\hbar\omega/2k_B T)}, \tag{11.69}$$

and performing the angular integration, one recovers (11.65). As another example, let us consider a ground-state atom ($T_A = 0$) moving in a "hot" field $T_F > 0$ with a small velocity. We can then put $N(\omega', T_A) = 0$ since for free space photons, $\omega' > 0$ (the positive-frequency part of the light cone in the $(\omega, \mathbf{k})$ space is a Lorentz-invariant set). Expanding in the Doppler shift, performing the angular integration and making a partial integration, one arrives at

$$\mathbf{f}(\mathbf{v}) \approx \mathbf{v} \frac{\hbar}{3\pi^2 \varepsilon_0 c^5} \int\limits_0^\infty d\omega \omega^2 \text{Im} \, \alpha^g(\omega) \partial_\omega [\omega^3 N(\omega, T_F)]. \tag{11.70}$$

Note that the function $\omega^3 N(\omega, T_F)$ has a positive (negative) slope for $\omega \lesssim k_B T_F/\hbar$ ($\omega \gtrsim k_B T_F/\hbar$), respectively. The velocity-dependent force thus accelerates the particle, $\mathbf{v} \cdot \mathbf{f} > 0$, if its absorption spectrum has a stronger weight at sub-thermal frequencies. This may happen for vibrational transitions in molecules and illustrates the unusual features that can happen in non-equilibrium situations. Drawing again the analogy to laser cooling, the radiative acceleration corresponds to the "anti-cooling" set-up where the laser beams have a frequency $\omega > \omega_{eg}$ ("blue detuning"). Indeed, we have just found that the peak of the thermal spectrum occurs on the blue side of the atomic absorption lines. As a rough estimate, consider the hydrogen atom (mass M) with transition dipoles of the order $|\mathbf{d}_{ag}| \sim ea_0$ (Bohr radius). If the atomic resonances are beyond the peak of the thermal spectrum, one gets from (11.70) a frictional damping time of the order of

$$\frac{1}{\Gamma_{bb}(T)} = \frac{Mv}{|\mathbf{f}(\mathbf{v})|} \sim \frac{10^{21}\text{s}}{(T/300\,\text{K})^5}, \tag{11.71}$$

which is longer than the age of the Universe. For estimates including resonant absorption where faster frictional damping may occur, see Ref. [82].

11.4.3.2 Radiative Friction Above a Surface

Near a surface, the fluctuations of the radiation field are distinct from free space, and are encoded in the surface-dependent Green function $\overleftrightarrow{\mathscr{G}}(L, \omega)$, see (11.16, 11.20). In addition, one has to take into account that the available photon momenta

differ, since also evanescent waves appear whose k-vectors have components larger than ω/c. All these properties can be expressed in terms of the electromagnetic Green tensor, assuming the field in thermal equilibrium. Let us consider for simplicity an atom with an isotropic polarizability tensor $\alpha_{ij} = \alpha\delta_{ij}$, moving at a non-relativistic velocity $\mathbf{v}$. From (118) in Ref. [87], one then gets a friction force

$$\hat{\mathbf{v}} \cdot \mathbf{f}(\mathbf{v}) = -\frac{2\hbar}{\pi} \int\limits_0^\infty \mathrm{d}\omega(-\partial_\omega N(\omega, T))\mathrm{Im}\alpha(\omega)(\hat{\mathbf{v}} \cdot \nabla)(\mathbf{v} \cdot \nabla')\mathrm{tr}\,\mathrm{Im}\,\overset{\leftrightarrow}{G}(\mathbf{r}, \mathbf{r}', \omega),$$

(11.72)

where the spatial derivatives are taken with respect to the two position variables of the Green tensor, and $\mathbf{r} = \mathbf{r}' = \mathbf{r}_A(t)$ is taken afterwards. This expression neglects terms of higher order in α that appear in the self-consistent polarizability (11.41); it can also be found from (25, 26) in Zurita Sanchez et al. [83].

Note that friction is proportional to the local density of field states, encoded in the imaginary part of the (electric) Green tensor $\overset{\leftrightarrow}{G}$. If the motion is parallel to a plane surface, the result only depends on the distance L and is independent of time. The friction force is comparable in magnitude to the free-space result (11.67) if the distance L is comparable or larger than the relevant wavelengths c/ω: the derivatives in (11.72) are then of the order $(\hat{\mathbf{v}} \cdot \nabla)(\mathbf{v} \cdot \nabla') \sim |\mathbf{v}|(\omega/c)^2$. At sub-wavelength distances, the non-retarded approximation for the Green tensor can be applied (see Table 11.1), and the previous expression becomes of the order of $|\mathbf{v}|/L^2$. The remaining integral is then similar to the temperature-dependent part of the atom–surface interaction discussed in Sect. 11.4.4.2 below. An order of magnitude estimate can be found in the non-retarded regime, using the approximate Green tensor of Table 11.1. For a metallic surface, the conductivity σ within the thermal spectrum is a relevant parameter; a typical value is $\sigma/\varepsilon_0 \sim 10^{16}\,\mathrm{s}^{-1}$. Taking the atomic polarizability of hydrogen as before, one gets a slight increase relative to the blackbody friction rate (11.71):

$$\Gamma(L, T) \sim \Gamma_{\mathrm{bb}}(T)\frac{\lambda_T^4}{L^4}\frac{c\varepsilon_0}{L\sigma} \sim 10^{-20}\,\mathrm{s}^{-1}\frac{(T/300\,\mathrm{K})^2}{(L/1\,\mu\mathrm{m})^5}, \quad (11.73)$$

but the effect is still negligibly small, even at distances in the nm range.

An expression that differs from (11.72) has been found by Scheel and Buhmann [81] who calculated the radiation force on a moving atom to first order in the velocity, and at zero temperature. Their analysis provides a splitting into resonant and non-resonant terms, similar to (11.61). For the ground state, the friction force is purely non-resonant and contains a contribution from the photonic mode density, similar to (11.72), and one from the Röntgen interaction that appears by evaluating the electric field in the frame co-moving with the atom. Another non-resonant friction force appears due to a velocity-dependent shift in the atomic resonance frequency, but it vanishes for ground-state atoms and for the motion

parallel to a planar surface. The remaining friction force becomes in the non-retarded limit and for a Drude metal

$$\mathbf{f}(\mathbf{v}) \approx -\frac{\mathbf{v}}{16\pi\varepsilon_0 L^5} \sum_{a > g} \frac{|\mathbf{d}^{ag}|^2 \omega_s \Gamma_a}{(\omega_{ag} + \omega_s)^3}, \tag{11.74}$$

where the sum $a > g$ is over excited states, the relevant dipole matrix elements are $|\mathbf{d}^{ag}|^2 = \sum_i |d_i^{ag}|^2$, Γ_a is the radiative width of the excited state (which also depends on L), and $\omega_s = \omega_p/\sqrt{2}$ the surface plasmon resonance in the non retarded limit. The fluctuations of the electromagnetic field are calculated here without taking into account the "back-action" of the atom onto the medium (see Ref. [85] and the discussion below). In order of magnitude, atomic and plasmon resonances are often comparable, $\omega_{ag} \sim \omega_s$. Taking hydrogen dipole elements, one thus gets a friction rate

$$\frac{|\mathbf{f}(\mathbf{v})|}{Mv} \approx \frac{\alpha_{\mathrm{fs}}^2}{3} \frac{\hbar\omega_s a_0^4}{ML^5 c} \sim \frac{10^{-16}\,\mathrm{s}^{-1}}{(L/1\mu\mathrm{m})^5}. \tag{11.75}$$

This is significantly larger than (11.73) and does not depend on temperature.

We briefly mention that the behaviour of friction forces in the limit of zero temperature ("quantum friction") has been the subject of discussion that is still continuing (see also the Chap. 13 by Dalvit et al. in this volume for further discussion on quantum friction). An early result of Teodorovich on the friction force between two plates, linear in $\mathbf{v}$ with a nonzero coefficient as $T \to 0$ [88], has been challenged by Harris and Schaich [85]. They point out that a charge or current fluctuation on one metallic plate can only dissipate by exciting electron-hole pairs in the other plate, but the cross-section for this process vanishes like T^2. This argument does not hold, however, for Ohmic damping arising from impurity scattering. In addition, Ref. [85] points out that the fluctuations of the atomic dipole should be calculated with a polarizability that takes into account the presence of the surface. This self-consistent polarizability has been discussed in Sect. 11.2.4 and reduces the friction force, in particular at short (non-retarded) distances. Carrying out the calculation for a metallic surface and in the non-retarded regime, Harris and Schaich find the scaling

$$\mathbf{f}(\mathbf{v}) \approx -\mathbf{v}\frac{\hbar\alpha_{\mathrm{fs}}^2}{L^{10}}\left(\frac{\alpha(0)c}{4\pi\varepsilon_0\omega_s}\right)^2, \tag{11.76}$$

where α_{fs} is the fine structure constant, $\alpha(0)$ is the static polarizability of the atom, and again ω_s the surface plasmon frequency. Note the different scaling with distance L compared to (11.74). Let us consider again $L = 100\,\mathrm{nm} - 1\,\mu\mathrm{m}$ for the ease of comparison, although shorter distances are required to get into the non-retarded regime. Taking the hydrogen polarizability and a surface plasmon at $\omega_s \sim 10^{16}\,\mathrm{s}^{-1}$, (11.76) gives a friction rate of the order $10^{-24}\,\mathrm{s}^{-1}(L/1\,\mu\mathrm{m})^{-10}$. This is about eight (three) orders of magnitude smaller that the estimate (11.75) at a distance $L = 1\,\mu\mathrm{m}$ (100 nm), respectively.

11.4.4 Non-equilibrium Field

A radiation field that is not in thermal equilibrium is a quite natural concept since under many circumstances, an observer is seeing radiation where the Poynting vector is non-zero (broken isotropy) and where the frequency spectrum is not given by the (observer's) temperature. The modelling of these fields can be done at various levels of accuracy: "radiative transfer" is a well-known example from astrophysics and from illumination engineering—this theory can be understood as a kinetic theory for a "photon gas". It is, in its simplest form, not a wave theory and therefore not applicable to the small length scales (micrometer and below) where atom–surface interactions are relevant. "Fluctuation electrodynamics" is a statistical description based on wave optics, developed by the school of S. M. Rytov [19, 89], and similar to optical coherence theory developed by E. Wolf and co-workers [25]. The main idea is that the radiation field is generated by sources whose spectrum is related to the local temperature and the material parameters of the radiating bodies. The field is calculated by solving the macroscopic Maxwell equations, where it is assumed that the matter response can be treated with linear response theory (medium permittivity or dielectric function $\varepsilon(\mathbf{x}, \omega)$ and permeability $\mu(\mathbf{x}, \omega)$). This framework has been used to describe the quantized electromagnetic field, as discussed by Knöll and Welsch and their co-workers [90], by the group of Barnett [91], see also the review paper [92]. Another application is radiative heat transfer and its enhancement between bodies that are closer than the thermal (Wien) wavelength, as reviewed in [87, 93]. The non-equilibrium heat flux between two bodies at different temperatures is naturally calculated from the expectation value of the Poynting vector.

In this section we review the atom–surface interaction in the out-of-equilibrium configuration similar to the one studied in [94]: the atom is close to a substrate hold at temperature T_S, the whole being enclosed in a "cell" with walls (called "environment") at temperature T_E. In the following we will only consider the electric atom–surface interaction and we will use the zero temperature atomic electric polarizability. In fact, the electric dipole transitions are mainly in the visible range and their equivalent in temperature (10^{3-4} K) are not achieved in the experiment. Therefore the atom does not participate in the thermal exchange and can be considered in its ground state.

11.4.4.1 Fluctuation Electrodynamics and Radiative Forces

A very simple non-equilibrium situation occurs when an atom is located near a "heated body" whose temperature is larger than its "surroundings" (see Fig. 11.3). As mentioned above, it is quite obvious that the Poynting vector of the radiation field does not vanish: there is radiative heat flux from the body into the surrounding space. This flux is accompanied by a radiative force on the atom that depends on the atomic absorption spectrum, but also on the angular distribution of
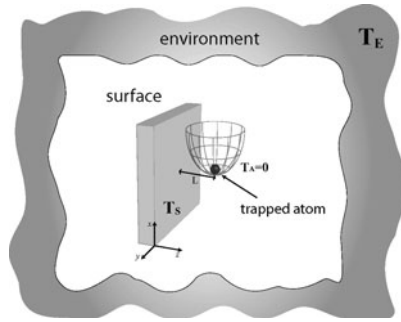
Fig. 11.3 Sketch of an atom–surface system with the field being out of thermal equilibrium. T_S is the temperature of the substrate and T_E is the temperature of the walls of the cell surrounding the atom–substrate system. If $T_S > T_E$, there is a nonzero radiative heat flux from the surface into the surrounding environment

radiated and re-scattered photons. The atom–photon interaction, in this case, does not derive from the gradient of a potential. The basic concept is that of the radiation force **F**; it is given by [43]

$$\mathbf{F}(\mathbf{r}) = \langle d_i \nabla E_i(\mathbf{r}) \rangle + \langle \mu_i \nabla B_i(\mathbf{r}) \rangle + \text{higher multipoles}, \qquad (11.77)$$

where we have written out only the contributions from the electric and magnetic dipole moments and the atom is assumed at rest at position **r**. (The generalization to a moving atom leads to the velocity-dependent forces discussed in Sect. 11.4.3.) As a general rule, the electric dipole is the dominant contribution for atoms whose absorption lines are in the visible range. (11.77) can be derived by averaging the Coulomb–Lorentz force over the charge and current distribution in the atom, assuming that the atomic size is small compared to the scale of variation (wavelength) of the electromagnetic field. The average $\langle \cdots \rangle$ is taken with respect to the quantum state of atom and field, and operator products are taken in symmetrized form.

The radiation force (11.77) can be evaluated with the scheme outlined in Sect. 11.2.1 where the operators **d** and **E**(**r**) are split into "freely fluctuating" and "induced" parts. Carrying this through for the contribution of field fluctuations, leads to an expression of the form

$$\langle d_i^{\text{ind}} \nabla E_i^{\text{free}}(\mathbf{r}) \rangle = \int \frac{d\omega \, d\omega'}{2\pi \, 2\pi} \alpha_{ij}(\omega) \langle E_j^{\text{free}}(\mathbf{r}, \omega) \nabla E_i^{\text{free}}(\mathbf{r}, \omega') \rangle, \qquad (11.78)$$

where the spatial gradient of a field autocorrelation function appears. In a non-equilibrium situation, the fluctuation-dissipation theorem of (11.16) cannot be applied, and this field correlation must be calculated in a different way. In a similar way, one gets

$$\langle d_i^{\text{free}} \nabla E_i^{\text{ind}}(\mathbf{r}) \rangle = \int \frac{d\omega \, d\omega'}{2\pi \, 2\pi} \nabla_1 G_{ij}(\mathbf{r}, \mathbf{r}, \omega') \langle d_i^{\text{free}}(\omega) d_j^{\text{free}}(\omega') \rangle, \qquad (11.79)$$

where the gradient $\nabla_1 G_{ij}$ is evaluated with respect to the first position coordinate of the Green function. This term requires some regularization because of the divergent Green function at coincident positions. The correlation function of the atomic dipole can be calculated in its stationary state which could be a thermal equilibrium state or not, as discussed in Sect. 11.4.2. In the case of an ultracold atomic gas, it is clear that the atom can be at an effectively much lower temperature compared to the macroscopic bodies nearby. This is consistent with the perturbation theory behind the operator splitting into fluctuating and induced parts. In global equilibrium, when both fluctuation spectra are given by the fluctuation-dissipation theorem (11.16, 11.17), it can be seen easily that the force reduces to the gradient of the equilibrium interaction potential (11.21).

Within Rytov's fluctuation electrodynamics, the fluctuating field is given in terms of its sources and the macroscopic Green function. Generalizing (11.14), one gets

$$E_i(\mathbf{r}, \omega) = \int \mathrm{d}^3 r' G_{ij}(\mathbf{r}, \mathbf{r}', \omega) P_j(\mathbf{r}', \omega) + \text{magnetization sources}, \qquad (11.80)$$

where we have not written down the contribution from the magnetization field that can be found in Ref. [39]. The polarization density $P_j(\mathbf{r}', \omega)$ describes the excitations of the material (dipole moment per unit volume). If the material is locally stationary, the polarization operator averages to zero and its correlations $\langle P_i(\mathbf{r}, \omega) P_j(\mathbf{r}', \omega') \rangle$ determine the field spectrum

$$\langle E_i(\mathbf{r}, \omega) E_j(\mathbf{r}', \omega') \rangle = \int \mathrm{d}^3 x \mathrm{d}^3 x' G_{ik}(\mathbf{r}, \mathbf{x}, \omega) G_{jl}(\mathbf{r}', \mathbf{x}', \omega') \langle P_k(\mathbf{x}, \omega) P_l(\mathbf{x}', \omega') \rangle, \tag{11.81}$$

Making the key assumption of local thermal equilibrium at the temperature $T(\mathbf{r})$, the source correlations are given by the *local version* of the fluctuation-dissipation theorem [89]:

$$\langle P_i(\mathbf{r}, \omega) P_j(\mathbf{r}', \omega') \rangle = 2\pi \hbar \delta(\omega + \omega') \delta_{ij} \delta(\mathbf{r} - \mathbf{r}') \coth \left(\frac{\hbar \omega}{2 k_B T(\mathbf{r})} \right) \mathrm{Im} \left[\varepsilon_0 \varepsilon(\mathbf{r}, \omega) \right], \tag{11.82}$$

where $\varepsilon(\mathbf{r}, \omega)$ is the (dimensionless) dielectric function of the source medium, giving the polarization response to a local electric field. The assumption of a local and isotropic (scalar) dielectric function explains the occurrence of the terms $\delta_{ij} \delta(\mathbf{r} - \mathbf{r}')$; this would not apply to ballistic semiconductors, for example, and to media with spatial dispersion, in general. The local temperature distribution $T(\mathbf{r})$ should in that case be smooth on the length scale associated with spatial dispersion (Fermi wavelength, screening length, mean free path). Similar expressions for random sources are known as "quasi-homogeneous sources" and are studied in the theory of partially coherent fields [25, Sect. 5.2].

If we define a polarization spectrum by

$$S_P(\mathbf{r}, \omega) = \hbar \coth\left(\frac{\hbar\omega}{2k_B T(\mathbf{r})}\right) \mathrm{Im}\left[\varepsilon_0 \varepsilon(\mathbf{r}, \omega)\right], \qquad (11.83)$$

the field correlation function (11.81) becomes

$$\langle E_i(\mathbf{r}, \omega) E_j(\mathbf{r}', \omega')\rangle = 2\pi\delta(\omega + \omega') \int \mathrm{d}^3 x \, G_{ik}^*(\mathbf{r}, \mathbf{x}, \omega') G_{jk}(\mathbf{r}', \mathbf{x}, \omega') S_P(\mathbf{x}, \omega'),$$
$$(11.84)$$

where (11.11) has been applied to the Green function. This expression was named "fluctuation-dissipation theorem of the second kind" by Eckhardt [47] who analyzed carefully its limits of applicability to non-equilibrium situations. Note that even if the sources are spatially decorrelated (the $\delta(\mathbf{r} - \mathbf{r}')$ in (11.82)), the propagation of the field creates spatial coherence, similar to the lab class diffraction experiment with a coherence slit. The spatial coherence properties of the field determine the order of magnitude of the field gradient that is relevant for the radiation force in (11.78).

Let us focus in the following on the correction to the atom–surface force due to the thermal radiation created by a "hot body". We assume that the atom is in its ground state and evaluate the dipole fluctuation spectrum in (11.79) at an atomic temperature $T_A = 0$. To identify the non-equilibrium part of the force, it is useful to split the field correlation spectrum in (11.78) into its zero-temperature part and a thermal contribution, using $\coth(\hbar\omega/2k_B T) = \mathrm{sign}(\omega)[1 + 2N(|\omega|, T)]$ with the Bose–Einstein distribution $N(\omega, T)$. The Rytov currents are constructed in such a way that at zero temperature, the fluctuation-dissipation theorem (11.16) for the field is satisfied. This can be achieved by allowing formally for a non-zero imaginary part $\mathrm{Im}\,\varepsilon(\mathbf{r}, \omega) > 0$ everywhere in space [48, 90], or by combining the radiation of sources located inside a given body and located at infinity [92, 95]. The two terms arising from dipole and field fluctuations then combine into a single expression where one recognizes the gradient of the Casimir–Polder potential Equation (11.21). This is discussed in detail in Refs. [33, 96]. The remaining part of the atom–surface force that depends on the body temperature is discussed now.

11.4.4.2 Radiation Force Near a Hot Body

Let us assume that the body has a homogeneous temperature $T(\mathbf{x}) = T_S$ and a spatially constant dielectric function. Using (11.84) and subtracting the $T = 0$ limit, the spectrum of the non-equilibrium radiation (subscript 'neq') can then be expressed by the quantity

$$\langle E_i(\mathbf{r}, \omega) E_j(\mathbf{r}', \omega')\rangle_{\mathrm{neq}} = 2\pi\delta(\omega + \omega') N(|\omega|, T_S) \hbar S_{ij}(\mathbf{r}, \mathbf{r}', \omega), \qquad (11.85)$$

$$S_{ij}(\mathbf{r}, \mathbf{r}', \omega) = \text{Im}\left[\varepsilon_0 \varepsilon(|\omega|)\right] \int\limits_S \text{d}^3x\, G_{ik}^*(\mathbf{r}, \mathbf{x}, \omega) G_{jk}(\mathbf{r}', \mathbf{x}, \omega), \qquad (11.86)$$

where the space integral is over the volume of the body. The tensor $S_{ij}(\mathbf{r}, \mathbf{r}', \omega)$ captures the material composition of the body and its geometry relative to the observation points.

Referring to the force due to field fluctuations in (11.78), let us assume for simplicity that the atomic polarizability is isotropic, $\alpha_{ij}(\omega) = \delta_{ij}\alpha(\omega)$. We combine the integrand over positive and negative frequencies to isolate dispersive and absorptive contributions ($\omega > 0$)

$$\begin{aligned}
&\alpha^*(\omega)\nabla_2 S_{ii}(\mathbf{r}, \mathbf{r}, \omega) + (\omega \mapsto -\omega) \\
&= \text{Re}[\alpha(\omega)]\nabla_{\mathbf{r}}[S_{ii}(\mathbf{r}, \mathbf{r}, \omega)] + 2\text{Im}[\alpha(\omega)]\text{Im}[\nabla_2 S_{ii}(\mathbf{r}, \mathbf{r}, \omega)],
\end{aligned} \qquad (11.87)$$

where ∇_2 is the gradient with respect to the second coordinate of S_{ij}, while $\nabla_{\mathbf{r}}$ differentiates both coordinates. This form highlights that the non-equilibrium force separates in two [97, 98] contributions that are familiar in laser cooling [99, 100]: a *dipole force* equal to the gradient of the electric energy density (proportional to $S_{ii}(\mathbf{r}, \mathbf{r}, \omega) \geq 0$). This is proportional to the real part of α and can be interpreted as the polarization energy of the atom in the thermal radiation field. The second term in (11.87) gives rise to *radiation pressure*, it is generally[1] proportional to the atomic absorption spectrum and the phase gradient of the field. The phase gradient can be identified with the local momentum of the emitted photons. By inspection of (11.86) for a planar surface, one indeed confirms that the radiation pressure force pushes the atom away from the thermal source. An illustration is given in Fig. 11.4 for a nanoparticle above a surface, both made from semiconductor. The dielectric function $\varepsilon(\omega)$ is of Lorentz–Drude form and uses parameters for SiC (see Ref. [33]). The arrows mark the resonance frequencies of transverse bulk phonon polaritons ω_T and of the phonon polariton modes of surface (ω_1) and particle (ω_2).

The radiation pressure force is quite difficult to observe with atomic transitions in the visible range because the peaks of the absorption spectrum are multiplied by the exponentially small Bose–Einstein factor $N(\omega_{ag}, T_S)$, even if the body temperature reaches the melting point. Alternative settings suggest polar molecules or Rydberg atoms [28] with lower transition energies. In addition, some experiments are only sensitive to force gradients (see Sect. 11.5), and it can be shown that the radiation pressure above a planar surface (homogeneous temperature, infinite lateral size) does not change with distance.

---

[1] Note that when the dressed polarizability is used instead of the bare one, the polarizability has an imaginary part even in the absence of absorption (see discussion at the end of Sect. 11.2.4). This is equivalent to include the effects of the "radiative reaction" in the dynamic of the dipole [97, 101, 102] as required by the conservation of energy and the optical theorem.
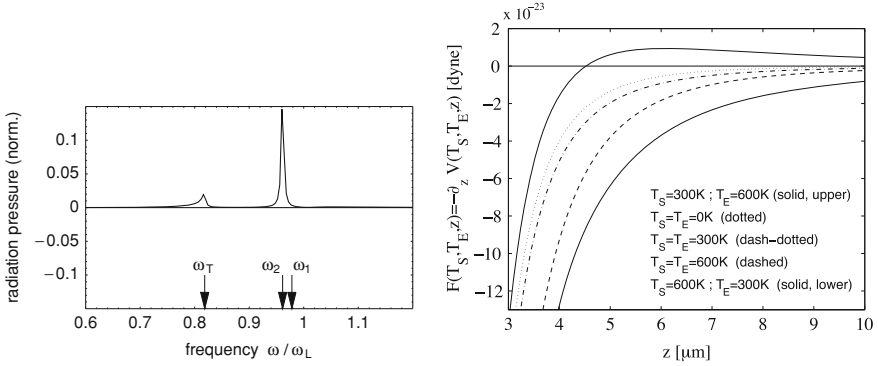
Fig. 11.4 *Left* spectrum of thermal radiation pressure force exerted on a small spherical particle above a planar substrate (positive = repulsive, does not depend on distance). The arrows mark the substrate and particle resonances at $\mathrm{Re}\,\varepsilon^{-1}(\omega_T) = 0$ (bulk phonon polariton) and $\mathrm{Re}\,\varepsilon(\omega_{1,2}) = -1, -2$ (surface and particle phonon polariton). The force spectrum is given by $\hbar N(\omega, T_S)$ times the second term in (11.87), and normalized to $(16/3)\hbar k_L(k_L a)^3 N(\omega, T_S)$ where a is the particle radius and $k_L = \omega_L/c$ the wavenumber of the longitudinal bulk polariton ($\mathrm{Re}\,\varepsilon(\omega_L) = 0$). *Right* theoretical calculation of the atom–surface force, in and out of thermal equilibrium, taken from Ref. [94], Fig. 11.2. The atom is Rubidium 87 in its electronic ground state, the surface is made of sapphire (SiO_2). Note the variation with temperature(s) of the non-equilibrium force, both in magnitude and in sign. A negative sign corresponds to an attractive interaction

For the evaluation of the dipole force, the same argument related to the field temperature can be applied so that the atomic polarizability in (11.87) is well approximated by its static value, $\mathrm{Re}\,\alpha(\omega) \approx \alpha(0)$. We thus find

$$\mathbf{F}_{\mathrm{neq}}^{\mathrm{dip}}(\mathbf{r}, T_S, T_E = 0) = -\nabla U_{\mathrm{neq}}^{\mathrm{dip}}(\mathbf{r}, T_S, T_E = 0), \qquad (11.88)$$

$$U_{\mathrm{neq}}^{\mathrm{dip}}(\mathbf{r}, T_S, T_E = 0) = -\alpha(0) \int\limits_0^\infty \frac{\mathrm{d}\omega}{2\pi} \hbar N(\omega, T_S) S_{ii}(\mathbf{r}, \mathbf{r}, \omega). \qquad (11.89)$$

11.4.4.3 General Non-Equilibrium Configuration and Asymptotic Behaviours

In the general case both T_S and T_E can be different from zero [94]. The total force will be the sum of $\mathbf{F}_{\mathrm{neq}}^{\mathrm{dip}}(\mathbf{r}, T_S, T_E = 0)$ given in the previous expression and of

$$\mathbf{F}_{\mathrm{neq}}^{\mathrm{dip}}(\mathbf{r}, T_S = 0, T_E) = \mathbf{F}_{\mathrm{eq}}^{\mathrm{dip}}(\mathbf{r}, T_E) - \mathbf{F}_{\mathrm{neq}}^{\mathrm{dip}}(\mathbf{r}, T_E, T_S = 0), \qquad (11.90)$$

that is the difference between thermal force at equilibrium at the temperature T_E and the force in (11.88) and (11.89) with T_S and T_E swapped. An illustration of the resulting force is given in Fig. 11.4 (right) for a planar surface. A large-distance

asymptote of the non-equilibrium interaction can be derived in the form [94, 103, 104]

$$L \gg \frac{\lambda_T}{\sqrt{\varepsilon(0) - 1}} : \qquad U_{\text{neq}}^{\text{dip}}(L, T_S, T_E) \approx -\frac{\pi}{12}\alpha(0)\frac{\varepsilon(0) + 1}{\sqrt{\varepsilon(0) - 1}}\frac{k_B^2(T_S^2 - T_E^2)}{\hbar c L^2},$$

$$(11.91)$$

where $\varepsilon(0) < \infty$ is the static dielectric constant. The previous expression is valid for dielectric substrates, see Ref. [94] for Drude metals. For $T_S = T_E$, this formula vanishes, and one ends with the "global equilibrium" result of (11.61).

Expression (11.91) shows that the configuration out of thermal equilibrium presents new features with respect to the equilibrium force. Indeed the force scales as the difference of the square of the temperatures and can be attractive or repulsive. For $T_E > T_S$ the force changes sign, going from attractive at small distance to repulsive at large distance (i.e. featuring a unstable equilibrium position in between), and it decays slower than the equilibrium configuration ($\propto L^{-4}$), leading therefore to a stronger force. This new feature was important for first measurement of the thermal component of the surface-atom surface (see next section). Moreover, when a gas of atoms is placed in front of the surface, the non-equilibrium interaction can lead to interesting non-additive effects [96, 105].

11.5 Measurements of the Atom–Surface Force with Cold Atoms

11.5.1 Overview

We do not discuss here the regime of distances comparable to the atomic scale where atomic beams are diffracted and reveal the crystallography of the atomic structure of the surface. We consider also that the atoms are kept away even from being physisorbed in the van der Waals well (a few nanometers above the surface). One is then limited to distances above approximately one micron (otherwise the attractive forces are difficult to balance by other means), but can take advantage of the techniques of laser cooling and micromanipulation and use even chemically very reactive atoms like the alkalis.

The first attempts to measure atom–surface interactions in this context go back to the sixties, using atomic beam set-ups. In the last 20 years, technological improvements have achieved the sensitivity required to detect with good accuracy and precision tiny forces. As examples, we mention the exquisite control over atomic beams provided by laser cooling [106, 107], spin echo techniques that reveal the quantum reflection of metastable noble gas beams [108, 109] (see also the Chap. 12 by DeKieviet et al. for detailed discussions on this topic), or the trapping of an ultracold laser-cooled gas in atom chip devices [5, 110]. In this

section we will briefly review some of the experiments which exploited cold atoms in order to investigate the Casimir–Polder force.

By using different techniques, it has been possible to measure the atom–surface interaction (atomic level shift, potential, force, or force gradient, depending on the cases) both at small ($0.1\,\mu m < L < \lambda_{opt} \approx 0.5\,\mu m$) and large ($L > 1\,\mu m$) distances. Because the interaction rapidly drops as the atom-surface separation becomes larger, the small-distance (van der Waals–London, (11.59)) regime at $L < \lambda_{opt}$ is somewhat easier to detect. Recall that in this limit, only the vacuum fluctuation of electromagnetic field are relevant, and retardation can be ignored. More recent experiments explored the weaker interaction in the Casimir–Polder regime (11.58), $\lambda_{opt} < L < \lambda_T$, where retardation effects are relevant, but thermal fluctuations still negligible. Also the Lifshitz–Keesom regime at $L > \lambda_T$ has been explored, where thermal fluctuations are dominant [see (11.60)]. The theory of Dzyaloshinskii, Lifshitz, and Pitaevski (DLP, [19,Chap.VIII]) encompasses the three regimes with crossovers that are illustrated in Fig. 11.1 for a Rubidium atom and a room temperature sapphire surface.

## 11.5.2 From van der Waals to Casimir–Polder: Equilibrium

Typically, experiments have been performed at room temperature, and at thermal equilibrium, and used several techniques to measure the interaction, usually of mechanical nature.

The van der Waals–London regime has been first explored by its effect on the deflection of an atomic beam passing close to a substrate [111–114]. Such kind of experiments were almost qualitative, and hardly in agreement with the theory. Subsequently, more accurate measurements of the atom–surface interaction in this regime have been done by using dielectric surfaces "coated" with an evanescent laser wave that repels the atoms (atom mirrors, [115]), by atom diffraction from transmission gratings [116, 117], by quantum reflection [108, 109], and by spectroscopic studies [106, 118].

The Casimir–Polder regime, where vacuum fluctuations of the electromagnetic field and the finite speed of light are relevant, was first studied experimentally in [107].[2] Here the force has been measured through an atomic beam deflection technique, which consists in letting an atomic beam (Na atoms in their ground state) pass across in a cavity made by two walls (gold plates), as one can see in Fig. 11.5. The atoms of the beam are drawn by the Casimir–Polder force to the walls, whose intensity depends on the atomic position within the cavity. Part of the atoms are deflected during their path and stick to the cavity walls without reaching

---

[2] Reprinted figures with permission from C. I. Sukenik, M. G. Boshier, D. Cho, V. Sandoghdar, and E. A. Hinds, Phys. Rev.Lett. **70**, 560 (1993). Copyright (1993) by the American Physical Society.
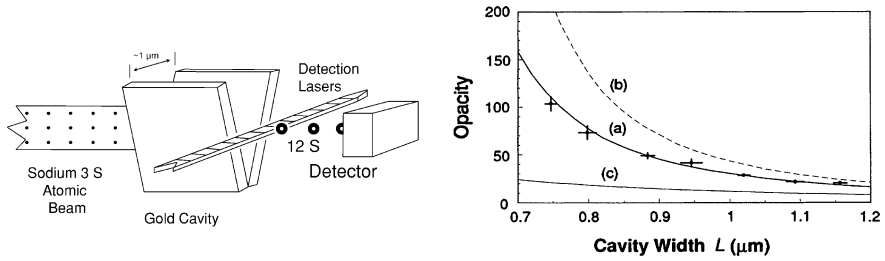
Fig. 11.5 (*left*) Scheme of the experiment of Sukenik and al, taken from Ref. [107]. An atomic beam enters a micron-sized gold cavity, and the flux of atoms emerging the cavity is detected and related to the atom–surface potential inside the cavity. (*right*) Measurement of the atom–surface interaction in the Casimir–Polder regime, in the experiment of [107], taken from the same paper. The opacity is proportional to the number of atoms which do not exit from the cavity, and is related to the atom–surface potential. The solid lines are the theoretical prediction based on: full DLP potential (**a**), van der Waals–London (*short-distance*) potential (**b**), and no atom–surface potential (**c**)

the end of the cavity. Only few atoms will pass the whole cavity, and their flux is measured and related to the atom–surface interaction in the cavity. Such a measurement is shown in Fig. 11.5, where the theoretical curves are based on atomic trajectories in the atom–surface potential that is assumed to be either of van der Waals-London or of Casimir–Polder form. The data are clearly consistent with the CP interaction, hence retardation already plays a role for typical distances in the range of 500 nm.

Subsequent measurements of the Casimir–Polder force have been done, among others, using the phenomenon of quantum reflection of ultra-cold atomic beams from a solid surface [108, 109]. In the experiment, a collimated atomic beam of metastable Neon atoms impinges on a surface (made of Silicon or some glass) at a glancing angle (very small velocity normal to the surface). In this regime, the de Broglie wave of the incident atoms must adapt its wavelength to the distance-dependent potential, and fails to do so because the potential changes too rapidly on the scale of the atomic wavelength. This failure forces the wave to be reflected, a quantum effect that would not occur in an otherwise attractive potential. In the limit of zero normal velocity (infinite wavelength), the reflection probability must reach 100%. The variation with velocity depends on the shape of the atom–surface potential and reveals retardation effects [119, 120]. In Fig. 11.6 is shown the measurement of quantum reflection performed by Shimizu [108].[3] In this case, the accuracy was not high enough to distinguish reliably between theoretical predictions. More recent data are shown in Fig. 12.5 of the chapter by DeKieviet et al. in this volume.

---

[3] Reprinted figure with permission from F. Shimizu, Phys. Rev. Lett. **86**, 987 (2001). Copyright (2001) by the American Physical Society.

Fig. 11.6 Reflectivity as a function of the normal incident velocity of Ne* atoms on a Si(1,0,0) surface, taken from Fig. 3 of [108]. The experimental points (*squares*) are plotted together with a theoretical line calculated using the approximate expression $V_{CP} = -C_4/[(d+a)d^3]$, where $C_4 = 6.8 \ 10^{-56} \text{Jm}^4$ and a is a fitting parameter
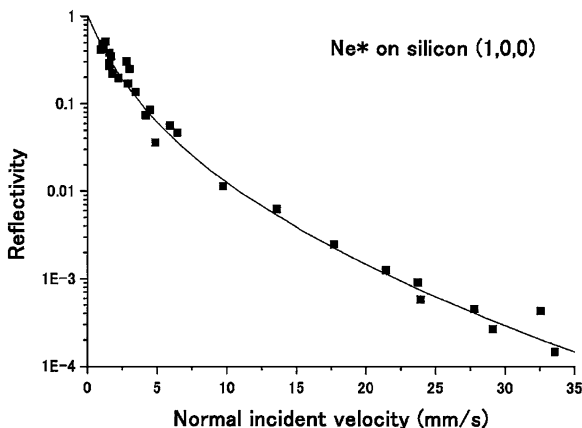
Fig. 11.7 Measured and theoretical prediction for the Casimir–Polder interaction, adapted from Fig. 3 of [121]. In the large figure theoretical calculation: asymptotic van der Waals–London (label "vdW"), asymptotic Casimir–Polder (label "ret"), and full theoretical curve (label "trans"). In the inset, measured data points are included: statistical and systematic errors are indicated by the error bars, and the gray shaded area, respectively
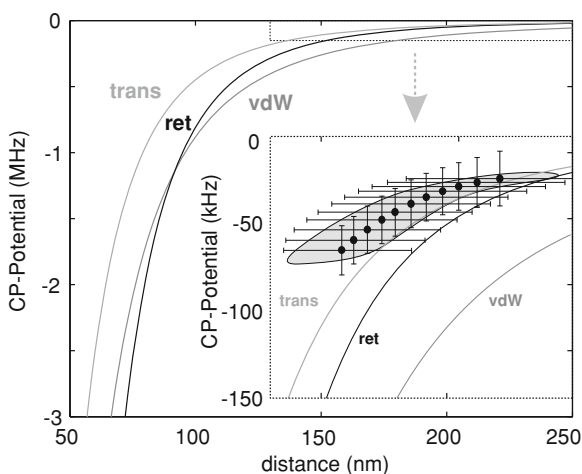
The crossover between the van der Waals and Casimir–Polder regimes has been recently measured by the group of C. Zimmermann and S. Slama [121], using the reflection of a cloud of ultracold atoms at an evanescent wave atomic mirror. This experiment improves previous data obtained by the A. Aspect group [115] into the crossover region. The data are shown in Fig. 11.7 where "vdW" and "ret" label the asymptotes van der Waals and Casimir–Polder potentials, respectively.[4] The full calculation (DLP theory) is labelled "trans" and show some deviation from both asymptotes in the crossover region. The data (shown with error bars) are clearly favoring the full (DPL) theory.

---

[4] Reprinted figure with permission from H. Bender, P.W. Courteille, C. Marzok, C. Zimmermann, and S. Slama, Phys. Rev. Lett. **104**, 083201 (2010). Copyright (2010) by the American Physical Society.
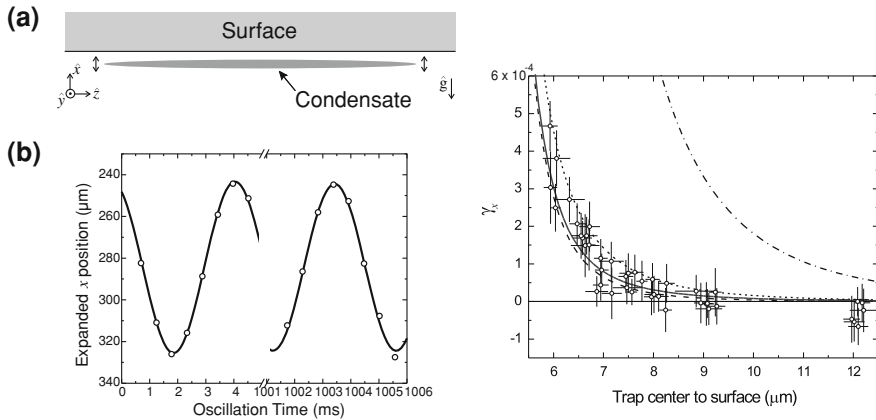
Fig. 11.8 (*left*) Scheme illustrating the experimental configuration in the E. Cornell group, taken from Fig. 1 of [122]. Typical arrangement of the condensate close to the surface. The cloud is formed by a few hundred thousand Rubidium 87 atoms, its axial length is $\sim 100\,\mu$m. The surface is made of fused silica. The coordinate axes and the direction of gravity are indicated (**a**). Typical data showing the center-of-mass (dipole) oscillation (*x*-direction normal to the surface). This is obtained after holding the BEC near the surface and then shifting it rapidly away from the surface; the "expanded position" is proportional to the velocity component v_x. (*right*) Measured and theoretical frequency of the BEC center-of-mass motion, relative to the nominal trap frequency ω_{trap} and normalized as $\gamma(x) = (\omega_{\text{cm}} - \omega_{\text{trap}})/\omega_{\text{trap}}$. Each data point represents a single measurement, with both statistical and systematic errors. The mean oscillation amplitude is $\approx 2.06\mu$m, and the typical size of the BEC (Thomas–Fermi radius) in the oscillation direction is $\approx 2.40\mu$m. Theory lines, calculated using theory from [124], consider the full atom-surface potential: $T = 0$ K (*dashed line*), $T = 300$ K (*solid line*) and $T = 600$ K (*dotted line*). No adjustable parameters have been used. The result of the van der Waals–London potential has been added (*dash-dotted line*) (**b**)

11.5.3 The Experiments of the E. Cornell Group

11.5.3.1 Lifshitz Regime

The atom–surface interaction in the Lifshitz regime has been explored in E. Cornell's group [5, 122]. Here a quantum degenerate gas in the Bose–Einstein condensed phase has been used as local sensor to measure the atom–surface interaction, similar to the work in V. Vuletić's group where smaller distances were involved [110]. The Cornell experiments use a Bose–Einstein condensate (BEC) of a few 10^5 ^{87}Rb atoms that are harmonically trapped at a frequency ω_{trap}. The trap is moved towards the surface of a sapphire substrate, as illustrated in Fig. 11.8.

Center-of-mass (dipole) oscillations of the trapped gas are then excited in the direction normal to the surface. In absence of atom–surface interaction, the frequency of the center-of-mass oscillation would correspond to the frequency of the trap: $\omega_{\text{cm}} = \omega_{\text{trap}}$. Close to the substrate, the atom–surface potential changes the effective trap frequency, shifting the center-of-mass frequency by a quantity $\gamma =$

$(\omega_{cm} - \omega_{trap})/\omega_{trap}$. The value of γ is related to the atom–surface force [4] and for small oscillation amplitudes we have:

$$\omega_{cm}^2 = \omega_{trap}^2 + \frac{1}{m} \int_{-R_z}^{R_z} dz\, n_0^z(z)\, \partial_z^2 \mathscr{F}(z), \tag{11.92}$$

where m is the atomic mass, $\mathscr{F}(z)$ is the atom–surface free energy in (11.21) (z is the direction normal to the surface), and $n_0^z(z)$ is the xy-integrated unperturbed atom density profile [4] that takes into account the finite size of the gas cloud. In the Thomas–Fermi approximation

$$n_0^z(z) = \frac{15}{16R_z}[1 - \left(\frac{z}{R_z}\right)^2]^2, \tag{11.93}$$

where R_z (typically of few microns) is the cloud radius along z, which depends on the chemical potential. In the comparison with the experiment, non-linear effects due to large oscillation amplitudes [4] may become relevant [122]. The experiment of Ref. [122] was performed at room temperature and succeeded in measuring the atom–surface interaction for the first time up to distances $L \approx 7\,\mu m$ (see Fig. 11.8). Although the relative frequency shift in (11.89) is only $\sim 10^{-4}$, the damping of this dipole oscillator is so weak that its phase can be measured even after hundreds of periods, (see Fig. 11.8 (left)). The same technique has been recently proposed to test the interaction between an atom and a non-planar surface [124, 125].

11.5.3.2 Temperature Dependence and Non-Equilibrium Force

The experiment of Ref. [122] did not reach the accuracy to discriminate between the theoretical predictions at $T = 0$ K and the $T = 300$ K, and a clear evidence of thermal effects was still missing. In this experiment there was no room to increase the temperature of the surface: at high temperatures some atoms thermally desorb from the walls of the cell, the vacuum in the cell degrades, resulting in the impossibility to produce a BEC. To overcome this experimental limitation a new configuration was studied, where only the surface temperature was increased: the quality of the vacuum was not affected because of the relatively small size of the substrate. The non-equilibrium theory of atom–surface interactions in this system was developed in Refs. [94, 96, 104, 105, 126], as outlined in Sect. 11.4. It predicts new qualitative and quantitative effects with respect to global equilibrium that are illustrated in Fig. 11.4 (right). The experimental measurement has been achieved in 2007 [5] and remains up to now the only one that has detected thermal effects of the electromagnetic dispersion interactions in this range of distances. A sketch of the experimental apparatus is given in Fig. 11.9, the experimental results in Fig. 11.10.

Fig. 11.9 Scheme of the experiment of Ref. [5] (from which the figure is taken), where atom–surface interactions out of thermal equilibrium have been measured
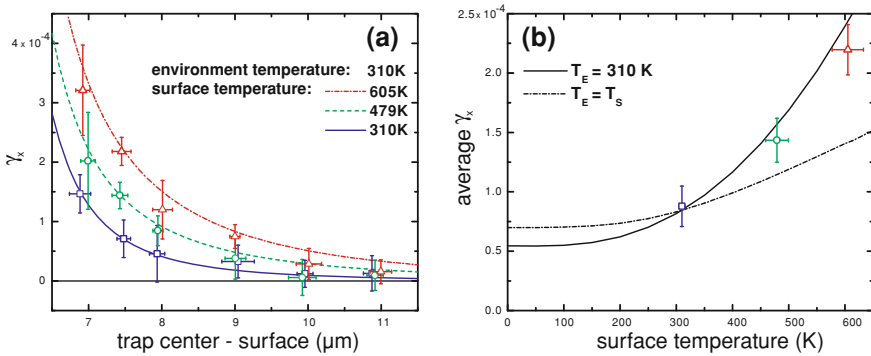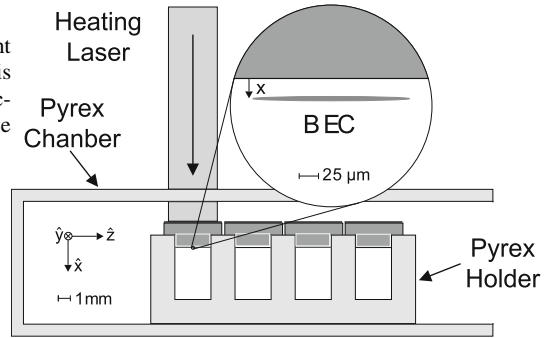
Fig. 11.10 Measured and theoretical frequency shift γ of the center-of-mass frequency ω_{cm} for a trapped atomic BEC (^{87}Rb atoms) close to surface (fused silica), in a system in and out of thermal equilibrium. The figure is taken from Fig. 4 of [5]. **a** The figure shows three sets of data and accompanying theoretical curves with no adjustable parameters for various substrate temperatures. Data are shown for different substrate temperatures: $T_S = 310$ K (*squares*), $T_S = 479$ K (*circles*), and $T_S = 605$ K (*triangles*). The environment temperature is maintained at $T_E = 310$ K. The error bars represent the total uncertainty (statistical and systematic) of the measurement. **b** Average values γ_x over the trap center–surface separations of 7.0, 7.5, and 8.0 μm, plotted versus substrate temperature. It is evident a clear increase in strength of the atom–surface interaction for elevated temperatures. The solid theory curve represents the non-equilibrium effect, while the dash–dotted theory curve represents the case of equal temperatures

11.5.3.3 Outlook

Precision measurements of the atom–surface interaction may shed light on the ongoing discussion about the temperature dependence of dispersion interactions with media that show absorption, like any conducting medium. It has been pointed out by Klimchitskaya and Mostepanenko [127] that if the small, but nonzero conductivity of the glass surface in the Cornell experiment [5, 122] had been taken into account, the Lifshitz–Keesom tail would involve an infinite static dielectric function, and hence deviate from a dielectric medium where $1 < \varepsilon(0) < \infty$. This

theoretical prediction would also be inconsistent with the data. This issue is related to similar problems that arise in the macroscopic Casimir interaction, see other chapters in this volume and Refs. [128–130] for reviews. In the atom–surface case, Pitaevskii has pointed out that a smooth crossover from a metal to a dielectric is obtained within a non-local description that takes into account electric screening in the surface (wave-vector-dependent dielectric function $\varepsilon(\mathbf{k}, \omega)$) [131] which Ref. [127] did not include.

New interesting experimental proposals have been presented in order to measure the atom–surface force with higher accuracy, essentially based on interferometric techniques. All of them deal with atoms trapped in a periodic lattice made by laser beams ("optical lattice" [132, 133]), and placed close to a substrate. Gradients in the potential across the lattice can be detected with coherent superposition states of atoms delocalized over adjacent lattice sites [7]. These gradients also induce Bloch oscillations through the reciprocal space of the lattice: if $\hbar q$ is the width of the Brillouin zone, the period τ_B of the Bloch oscillations is [6]

$$\frac{1}{\tau_B} = \frac{\overline{-\partial_L U}}{\hbar q}. \tag{11.94}$$

where the average (overbar) is over the cloud size in the lattice. The atom–surface interaction would, in fact, shift the Bloch period by a relative amount of $10^{-4} \ldots 10^{-3}$ if the main force is gravity and the atoms are at a distance $L \approx 5\,\mu m$ [105]. Distance-dependent shifts in atomic clock frequencies have also been proposed [134]. They arise from the differential energy shift of the two atomic states which are related to the difference in polarizabilities. Finally, a corrugated surface produces a periodic Casimir–Polder potential that manifests itself by a band gap in the dispersion relation of the elementary excitations of the BEC (Bogoliubov modes). The spectrum of these modes is characterized by a dynamic structure factor that can be detected by the Bragg scattering of a pair of laser beams [135].

11.6 Conclusion

In this chapter, we have outlined a quantum theory of fluctuations, focussing on "discrete systems" like atoms or nanoparticles and on a quantized field. As atoms interact with the electromagnetic field, the fluctuations of the two entities get correlated, and this becomes manifest in forces, energy shifts, and damping rates. We have presented a formalism where these radiative interactions are described by response functions (polarizabilities, Green functions), and thermodynamics enters via the fluctuation-dissipation theorem, a powerful generalization of the Einstein relation familiar from Brownian motion. These interactions have been explored recently over an extended range of distances between atoms and macroscopic bodies, using experimental techniques from laser cooling and ultracold atom manipulation. Atom-surface interactions are setting now non-trivial limitations for

the stability of micro-traps and nano-devices, as their dimensions are reduced. Non-equilibrium situations ("cold atoms near a hot body") are quite common in these settings, and we have outlined in this chapter the corresponding fluctuation theory based on local thermodynamic equilibrium. For atom–surface interactions, this theory is relatively simple to formulate since to a good approximation, atoms are "probe particles" that do not affect the quantum state of the field (and of the macroscopic surroundings). Still, subtle issues have emerged in controversies, both long standing and more recent, that are related to the choice of placing the "cut" between "system" (dynamically responding) and "bath" (in thermodynamic equilibrium). We anticipate that experimental and theoretical advances in the near future will help to resolve these issues within the challenging realm of open quantum systems.

References

1. Diedrich, F., Bergquist, J.C., Itano, M.W., Wineland, D.J.: Laser cooling to the zero-point energy of motion. Phys. Rev. Lett. **62**, 403 (1989)
2. Meekhof, D.M., Monroe, C., King, B.E., Itano, W.M., Wineland, D.J: Generation of nonclassical motional states of a trapped ion. Phys. Rev. Lett. **76**, 1796 (1996)
3. Pitaevskii, L.P., Stringari, S.: Bose–Einstein Condensation, 116 of International Series of Monographs on Physics. Clarendon Press, Oxford (2003)
4. Antezza, M., Pitaevskii, L.P., Stringari, S.: Effect of the Casimir–Polder force on the collective oscillations of a trapped Bose–Einstein condensate. Phys. Rev. A. **70**, 053619 (2004)
5. Obrecht, J.M., Wild, R.J., Antezza, M., Pitaevskii, L.P., Stringari, S., Cornell, E.A.: Measurement of the temperature dependence of the Casimir–Polder force. Phys. Rev. Lett. **98**, 063201 (2007)
6. Carusotto, I., Pitaevskii, L., Stringari, S., Modugno, G., Inguscio, M.: Sensitive measurement of forces at micron scale using bloch oscillations of ultracold atoms. Phys. Rev. Lett. **95**, 093202 (2005)
7. Wolf, P., Lemonde, P., Lambrecht, A., Bize, S., Landragin, A., Clairon, A.: From optical lattice clocks to the measurement of forces in the Casimir regime. Phys. Rev. A. **75**, 063608 (2007)
8. Sorrentino, F., Alberti, A., Ferrari, G., Ivanov, V.V., Poli, N., Schioppo, M., Tino, G.M.: Quantum sensor for atom–surface interactions below 10 μm. Phys. Rev. A. **79**, 013409 (2009)
9. Onofrio, R.: Casimir forces and non-Newtonian gravitation. New J. Phys. **8**, 237 (2006)
10. Folman, R., Krüger, P., Schmiedmayer, J., Denschlag, J.H., Henkel, C.: Microscopic atom optics: from wires to an atom chip. Adv. At. Mol. Opt. Phys. **48**, 263 (2002)
11. Fortágh, J., Zimmermann, C.: Magnetic microtraps for ultracold atoms. Rev. Mod. Phys. **79**, 235 (2007)
12. Reichel, J., Hänsel, W., Hänsch, T.W.: Atomic micromanipulation with magnetic surface traps. Phys. Rev. Lett. **83**, 3398 (1999)

13. Folman, R., Krüger, P., Cassettari, D., Hessmo, B., Maier, T., Schmiedmayer, J.: Controlling cold atoms using nanofabricated surfaces: atom chips. Phys. Rev. Lett. **84**, 4749 (2000)
14. Ott, H., Fortagh, J., Schlotterbeck, G., Grossmann, A., Zimmermann, C.: Bose–Einstein condensation in a surface microtrap. Phys. Rev. Lett. **87**, 230401 (2001)
15. Roux, C., Emmert, A., Lupascu, A., Nirrengarten, T., Nogues, G., Brune, M., Raimond, J.-M., Haroche, S.: Bose–Einstein condensation on a superconducting atom chip. Europhys. Lett. **81**(56004), 6 (2008)
16. Cano, D., Kasch, B., Hattermann, H., Kleiner, R., Zimmermann, C., Koelle, D., Fortágh, J.: Meissner effect in superconducting microtraps. Phys. Rev. Lett. **101**, 183006 (2008)
17. Müller, T., Zhang, B., Fermani, R., Chan, K.S., Wang, Z.W., Zhang C.B., Lim M.J., Dumke, R.: Trapping of ultra-cold atoms with the magnetic field of vortices in a thin-film superconducting micro-structure. New J. Phys. **12**, 043016 (2010)
18. Parsegian, V.A.: van der Waals Forces—A Handbook for Biologists, Chemists, Engineers, and Physicists. Cambridge University Press, New York (2006)
19. Lifshitz, E.M., Pitaevskii, L.P.: Statistical Physics (Part 2), 9 of Landau and Lifshitz Course of Theoretical Physics. 2nd ed. Pergamon, Oxford (1980)
20. Margenau, H.: van der Waals forces. Rev. Mod. Phys. **11**, 1 (1939)
21. London, F.: Zur Theorie und Systematik der Molekularkräfte. Z. Physik. **63**, 245 (1930)
22. Verweey, E., Overbeek, J.: Theory of the Stability of Lyophobic Colloids. Elsevier Science Publishers, Amsterdam (1948)
23. Casimir, H.B., Polder, D.: The Influence of retardation on the London-van der Waals forces. Phys. Rev. **73**, 360 (1948)
24. Dzyaloshinskii, I.E., Lifshitz, E.M., Pitaevskii, L.P.: General theory of van der Waals' forces. Sov. Physics Usp. **4**, 153 (1961)
25. Mandel, L., Wolf, E.: Optical Coherence and Quantum Optics. Cambridge University Press, Cambridge (1995)
26. Linder, B.: van der Waals interaction potential between polar molecules. Pair Potential and (Nonadditive) Triple Potential. J. Chem. Phys. **40**, 2003 (1964)
27. Haakh, H., Intravaia, F., Henkel, C., Spagnolo, S., Passante, R., Power, B., Sols, F.: Temperature dependence of the magnetic Casimir–Polder interaction. Phys. Rev. A **80**, 062905 (2009)
28. Ellingsen, S.A., Buhmann, S.Y., Scheel, S.: Temperature-invariant Casimir–Polder forces despite large thermal photon numbers. Phys. Rev. Lett. **104**, 223003 (2010)
29. Dalibard, J., Dupont-Roc, J., Cohen-Tannoudji, C.: Vacuum fluctuations and radiation reaction: identification of their respective contributions. J. Physique (France) **43**, 1617 (1982)
30. Dalibard, J., Dupont-Roc, J., Cohen-Tannoudji, C.: Dynamics of a small system coupled to a reservoir: reservoir fluctuations and self-reaction. J. Physique (France) **45**, 637 (1984)
31. Callen, H.B., Welton, T.A.: Irreversibility and generalized noise. Phys. Rev. **83**, 34 (1951)
32. Meschede, D., Jhe, W., Hinds, E.A.: Radiative properties of atoms near a conducting plane: an old problem in a new light. Phys. Rev. A **41**, 1587 (1990)
33. Henkel. C., Joulain. K., Mulet.J.-P., Greffet.J.-J.: Radiation forces on small particles in thermal near fields. J. Opt. A: Pure Appl. Opt. **4**, S109 (2002), special issue "Electromagnetic Optics" (EOS Topical Meeting, Paris 26–30 August 2001)
34. Novotny, L., Henkel, C.: van der Waals versus optical interaction between metal nanoparticles. Opt. Lett. **33**, 1029 (2008)
35. McLachlan, A.D.: Retarded dispersion forces between molecules. Proc. R. Soc. London A. **271**, 387 (1963)
36. Wylie, J.M., Sipe, J.E.: Quantum electrodynamics near an interface. II. Phys. Rev. A. **32**, 2030 (1985)
37. Milonni, P.W.: The Quantum Vacuum. Academic Press Inc., San Diego (1994)
38. Sols, F., Flores, F.: Dynamic interactions between a charge or an atom and a metal surface. Solid State Commun. **42**, 687 (1982)

39. Buhmann, S.Y., Welsch, D.-G.: Dispersion forces in macroscopic quantum electrodynamics. Progr. Quantum Electr. **31**, 51 (2007)
40. Bezerra, V.B., Klimchitskaya, G.L., Mostepanenko, V.M., Romero, C.: Lifshitz theory of atom-wall interaction with applications to quantum reflection. Phys. Rev. A. **78**, 042901 (2008)
41. Bimonte, G.: Bohr-van Leeuwen theorem and the thermal Casimir effect for conductors. Phys. Rev. A. **79**, 042107 (2009)
42. Skagerstam, B.-S., Rekdal, P.K., Vaskinn, A.H.: Theory of Casimir–Polder forces. Phys. Rev. A. **80**, 022902 (2009)
43. Jackson, J.D.: Classical Electrodynamics. John Wiley and Sons Inc, New York, Berlin u.a., (1975) XIX, 938 S
44. Huttner, B., Barnett, S.M.: Dispersion and loss in a Hopfield dielectric. Europhys. Lett. **18**, 487 (1992)
45. Barnett, S.M., Huttner, B., Loudon, R., Matloob, R.: Decay of excited atoms in absorbing dielectrics. J. Phys. B: Atom. Mol. Opt. Phys. **29**, 3763 (1996)
46. Agarwal, G.S.: Quantum electrodynamics in the presence of dielectrics and conductors. I. electromagnetic-field response functions and black-body fluctuations in finite geometries. Phys. Rev. A. **11**, 230 (1975)
47. Eckhardt, W.: First and second fluctuation-dissipation-theorem in electromagnetic fluctuation theory. Opt. Commun. **41**, 305 (1982)
48. Eckhardt, W.: Macroscopic theory of electromagnetic fluctuations and stationary radiative heat transfer. Phys. Rev. A. **29**, 1991 (1984)
49. Rytov, S.M.: Theory of Electrical Fluctuations and Thermal Radiation. Publishing House, Academy of Sciences USSR (1953)
50. Matsubara, T.: A New approach to quantum statistical mechanics. Prog. Theor. Phys. **14**, 351 (1955)
51. Håkanson, U., Agio, M., Kühn, S., Rogobete, L., Kalkbrenner, T., Sandoghdar, V.: Coupling of plasmonic nanoparticles to their environments in the context of van der Waals—Casimir interactions. Phys. Rev. B. **77**, 155408 (2008)
52. Klimov, V., Lambrecht, A.: Plasmonic nature of van der Waals forces between nanoparticles. Plasmonics. **4**, 31 (2009)
53. Mie, G.: Beiträge zur Optik trüber Medien, speziell kolloidaler Metallösungen. Ann. Phys. **330**, 377 (1908)
54. Born, M., Wolf, E.: Principles of Optics. seventh ed. Cambridge University Press, Cambridge. (1999)
55. Feinberg, G., Sucher, J.: General form of the Van der Waals interaction: a model-independent approach. Phys. Rev. A. **2**, 2395 (1970)
56. Babb, J.F.: Long-range atom–surface interactions for cold atoms. J. Phys. Conf. Series. **19**, 1 (2005)
57. Renne, M.J.: Microscopic theory of retarded van der Waals forces between macroscopic dielectric bodies. Physica. **56**, 125 (1971)
58. Renne, M.J.: Retarded van der Waals interaction in a system of harmonic oscillators. Physica **53**, 193 (1971)
59. Davies, B.: Calculation of van der Waals forces from dispersion relations. Chem. Phys. Lett. **16**, 388 (1972)
60. Mahanty, J., Ninham, B.W.: Dispersion forces between oscillators: a semi-classical treatment. J. Phys. A: Gen. Phys. **5**, 1447 (1972)
61. Mahanty, J., Ninham, B.W.: Boundary effects on the dispersion force between oscillators. J. Phys. A: Math. Nucl. Gen. **6**, 1140 (1973)
62. Ford, G.W., Lewis, J.T., O'Connell, R.F.: Quantum oscillator in a blackbody radiation field. Phys. Rev. Lett. **55**, 2273 (1985)
63. Ford, L.H.: Spectrum of the Casimir effect. Phys. Rev. D **38**, 528 (1988)
64. Agarwal, G.S.: Quantum electrodynamics in the presence of dielectrics and conductors. I. Electromagnetic-field response functions and black-body fluctuations in finite geometries. Phys. Rev. A **11**, 230 (1975)

65. Wylie, J.M., Sipe, J.E.: Quantum electrodynamics near an interface. Phys. Rev. A **30**, 1185 (1984)
66. Sondheimer, E.H.: The mean free path of electrons in metals. Adv. Phys. **1**, 1 (1952)
67. Henkel, C., Pötting, S., Wilkens, M.: Loss and heating of particles in small and noisy traps. Appl. Phys. B **69**, 379 (1999)
68. Kittel, C.: Introduction to Solid State Physics. 7th ed. John Wiley and Son Inc., New York (1996)
69. Henkel, C.: Magnetostatic field noise near metallic surfaces. Eur. Phys. J. D **35**, 59 (2005), topical issue on Atom chips: manipulating atoms and molecules with microfabricated structures
70. Schrieffer, J.R.: (1999) Theory of Superconductivity (Perseus Books, Reading MA)
71. Joulain, K., Carminati, R., Mulet, J.-P., Greffet, J.-J.: Definition and measurement of the local density of electromagnetic states close to an interface. Phys. Rev. B **68**, 245405 (2003)
72. Philbin, T.G., Leonhardt, U.: No quantum friction between uniformly moving plates. New J. Phys. **11**(033035), 18 (2009)
73. Pendry, J.B.: Quantum friction—fact or fiction? New J. Phys. **12**, 033028 (2010)
74. Leonhardt, U.: Comment on quantum friction—fact or fiction? New J. Phys. **12**, 068001 (2010)
75. McLachlan, A.D.: Retarded dispersion forces between molecules. Proc. R. Soc. London A **271**, 387 (1963)
76. Gorza, M.P., Ducloy, M.: Van der Waals interactions between atoms and dispersive surfaces at finite temperature. Eur. Phys. J. D **40**, 343 (2006)
77. Einstein, A.: Zur Quantentheorie der Strahlung. Physik. Zeitschr. **18**, 121 (1917)
78. Wilkens, M.: Spurious velocity dependence of free-space spontaneous emission. Phys. Rev. A **47**, 671 (1993)
79. Wilkens, M.: Significance of Röntgen current in quantum optics: spontaneous emission of moving atoms. Phys. Rev. A **49**, 570 (1994)
80. Wilkens, M.: Quantum phase of a moving dipole. Phys. Rev. Lett. **72**, 5 (1994)
81. Scheel, S., Buhmann, S.Y.: Casimir–Polder forces on moving atoms. Phys. Rev. A **80**, 042902 (2009)
82. Mkrtchian, V., Parsegian, V.A., Podgornik, R., Saslow, W.M.: Universal Thermal Radiation Drag on Neutral Objects. Phys. Rev. Lett. **91**, 220801 (2003)
83. Zurita-Sánchez, J.R., Greffet, J.-J., Novotny, L.: Friction forces arising from fluctuating thermal fields. Phys. Rev. A **69**, 022902 (2004)
84. Kleppner, D.: Rereading Einstein on Radiation. Physics Today (Feb 2005) p. 30
85. Schaich, W.L., Harris, J.: Dynamic corrections to van der Waals potentials. J. Phys. F: Metal Phys. **11**, 65 (1981)
86. Dedkov, G.V., Kyasov, A.A.: Tangential force and heating rate of a neutral relativistic particle mediated by equilibrium background radiation. Nucl. Instr. Meth. Phys. Res. B **268**, 599 (2010)
87. Volokitin, A.I., Persson, B.N.J.: Near-field radiative heat transfer and noncontact friction. Rev. Mod. Phys. **79**, 1291 (2007)
88. Teodorovich, E.V.: On the Contribution of Macroscopic van der Waals Interactions to frictional force. Proc. R. Soc. London A **362**, 71 (1978)
89. Rytov, S.M., Kravtsov, Y.A., Tatarskii, V.I.: Elements of Random Fields, 3 of Principles of Statistical Radiophysics. (Springer, Berlin) (1989)
90. Knöll, L., Scheel, S., Welsch, D.-G.: In: Peřina, J. (ed) Coherence and statistics of photons and atoms, John Wiley & Sons. Inc., New York (2001)
91. Barnett. S.M.: (1997) . In: Quantum fluctuations. Les Houches, Session LXIII, 1995, edited by S. Reynaud, E. Giacobino, and J. Zinn-Justin (Elsevier, Amsterdam) 137–179
92. Henry, C.H., Kazarinov, R.F.: Quantum noise in photonics. Rev. Mod. Phys. **68**, 801 (1996)
93. Joulain, K., Mulet, J.-P., Marquier, F., Carminati, R., Greffet, J.-J.: Surface electromagnetic waves thermally excited: Radiative heat transfer, coherence properties and Casimir forces revisited in the near field. Surf. Sci. Rep. **57**, 59 (2005)

94. Antezza, M., Pitaevskii, L.P., Stringari, S.: New asymptotic behaviour of the surface-atom force out of thermal equilibrium. Phys. Rev. Lett. **95**, 113202 (2005)
95. Savasta, S., Stefano, O.D., Girlanda, R.: Light quantization for arbitrary scattering systems. Phys. Rev. A **65**, 043801 (2002)
96. Antezza, M., Pitaevskii, L.P., Stringari, S., Svetovoy, V.B.: Casimir–Lifshitz force out of thermal equilibrium. Phys. Rev. A **77**, 022901 (2008)
97. Chaumet, P.C., Nieto-Vesperinas, M.: Time-averaged total force on a dipolar sphere in an electromagnetic field. Opt. Lett. **25**, 1065 (2000)
98. Arias-González, J.R., Nieto-Vesperinas, M.: Optical forces on small particles: attractive and repulsive nature and plasmon-resonance conditions. J. Opt. Soc. Am. A **20**, 1201 (2003)
99. Dalibard, J., Cohen-Tannoudji, C.: Dressed-atom approach to atomic motion in laser light: the dipole force revisited. J. Opt. Soc. Am. B **2**, 1707 (1985)
100. Cohen-Tannoudji, C., Dupont-Roc, J., Grynberg, G.: Atom–photon interactions. Wiley, New York (1998)
101. Draine, B.: The discrete-dipole approximation and its application to interstellar graphite grains. Astrophys. J. **333**, 848 (1988)
102. Milonni, P.W., Boyd, R.W.: Momentum of Light in a Dielectric Medium. Adv. Opt. Photon. **2**, 519 (2010)
103. Antezza, M.: Surface–atom force out of thermal equilibrium and its effect on ultra-cold atoms force out of thermal equilibrium and its effect on ultra-cold atoms. J. Phys. A: Math. Theor. **39**, 6117 (2006)
104. Pitaevskii, L.P.: Long-distance behaviour of the surface-atom Casimir–Polder force out of thermal equilibrium. J. Phys. A: Math. Gen. **39**, 6665 (2006)
105. Antezza, M., Pitaevskii, L.P., Stringari, S., Svetovoy, V.B.: Casimir–Lifshitz force out of thermal equilibrium and asymptotic non-additivity. Phys. Rev. Lett. **97**, 223203 (2006)
106. Sandoghdar, V., Sukenik, C.I., Hinds, E.A., Haroche, S.: Direct measurement of the van der Waals interaction between an atom and its images in a micron-sized cavity. Phys. Rev. Lett. **68**, 3432 (1992)
107. Sukenik, C.I., Boshier, M.G., Cho, D., Sandoghdar, V., Hinds, E.A.: Measurement of the Casimir–Polder force. Phys. Rev. Lett. **70**, 560 (1993)
108. Shimizu, F.: Specular reflection of very slow metastable neon atoms from a solid surface. Phys. Rev. Lett. **86**, 987 (2001)
109. Druzhinina, V., DeKieviet, M.: Experimental Observation of Quantum Reflection far from Threshold. Phys. Rev. Lett. **91**, 193202 (2003)
110. Lin, Y.-J., Teper, I., Chin, C., Vuletić, V.: Impact of Casimir–Polder potential and Johnson noise on Bose–Einstein condensate stability near surfaces. Phys. Rev. Lett. **92**, 050404 (2004)
111. Raskin, D., Kusch, P.: Interaction between a Neutral Atomic or Molecular Beam and a Conducting Surface. Phys. Rev. **179**, 712 (1969)
112. Shih, A., Raskin, D., Kusch, P.:Investigation of the interaction potential between a neutral molecule and a conducting surface. Phys. Rev. A **9**, 652 (1974)
113. Shih, A., Parsegian, V.A.: Van der Waals forces between heavy alkali atoms and gold surfaces: Comparison of measured and predicted values. Phys. Rev. A **12**, 835 (1975)
114. Anderson, A., Haroche, S., Hinds, E.A., Jhe, W., Meschede, D., Moi, L.: Reflection of thermal Cs atoms grazing a polished glass surface. Phys. Rev. A **34**, 3513 (1986)
115. Landragin, A., Courtois, J.-Y., Labeyrie, G., Vansteenkiste, N., Westbrook C.I., Aspect, A.: Measurement of the van der Waals force in an atomic mirror. Phys. Rev. Lett. **77**, 1464 (1996)
116. Grisenti, R.E., Schöllkopf, W., Toennies, J.P., Hegerfeldt ,G.C., Köhler, T.: Determination of atom–surface van der Waals potentials from transmission-grating diffraction intensities. Phys. Rev. Lett. **83**, 1755 (1999)
117. Brühl, R., Fouquet, P., Grisenti R.E., Toennies, J.P., Hegerfeldt, G.C., Kohler, T., Stoll, M., Walter, C.: The van der Waals potential between metastable atoms and solid surfaces: novel diffraction experiments vs. theory. Europhys. Lett. **59**, 357 (2002)

118. Fichet, M., Dutier, G., Yarovitsky, A., Todorov, P., Hamdi, I., Maurin, I., Saltiel, S., Sarkisyan, D., Gorza, M.-P., Bloch, D. Ducloy, M.: Exploring the van der Waals atom–surface attraction in the nanometric range. Europhys. Lett. **77**, 54001 (2007)
119. Côté, R., Segev, B., Raizen, M.G.: Retardation effects on quantum reflection from an evanescent-wave atomic mirror. Phys. Rev. A **58**, 3999 (1998)
120. Friedrich, H., Jacoby, G., Meister, C.G.: Quantum reflection by Casimir–van der Waals potential tails. Phys. Rev. A **65**, 032902 (2002)
121. Bender, H., Courteille, P.W., Marzok, C., Zimmermann, C., Slama, S.: Direct measurement of intermediate-range Casimir–Polder potentials. Phys. Rev. Lett. **104**, 083201 (2010)
122. Harber, D.M., Obrecht, J.M., McGuirk, J.M., Cornell, E.A.: Measurement of the Casimir–Polder force through center-of-mass oscillations of a Bose–Einstein condensate. Phys. Rev. A **72**, 033610 (2005)
123. Antezza, M., Pitaevskii, L.P., Stringari, S.: Effect of the Casimir–Polder force on the collective oscillations of a trapped Bose–Einstein condensate. Phys. Rev. A **70**, 053619 (2004)
124. Dalvit, D.A.R., Lamoreaux, S.K.: Contribution of drifting carriers to the Casimir–Lifshitz and Casimir–Polder interactions with semiconductor materials. Phys. Rev. Lett. **101**, 163203 (2008)
125. Messina, R., Dalvit, D.A.R., Neto, P.A.M., Lambrecht, A., Reynaud, S.: Dispersive interactions between atoms and nonplanar surfaces. Phys. Rev. A **80**, 022119 (2009)
126. M. Antezza, Ph.D. thesis, University of Trento, 2006
127. Klimchitskaya, G.L., Mostepanenko, V.M.: Conductivity of dielectric and thermal atom—wall interaction. J. Phys. A. Math. Gen. **41**, 312002(F) (2008)
128. Brown-Hayes, M., Brownell, J.H., Dalvit, D.A.R., Kim, W.J., Lambrecht, A., Lombardo, F.C., Mazzitelli, F.D., Middleman, S.M., Nesvizhevsky, V.V., Onofrio, R., Reynaud, S.: Thermal and dissipative effects in Casimir physics. J. Phys. A. Math. Gen. **39**, 6195 (2006)
129. Klimchitskaya, G.L., Mohideen, U., Mostepanenko, V.M.: The Casimir force between real materials: experiment and theory. Rev. Mod. Phys. **81**, 1827 (2009)
130. Milton, K.A.: Recent developments in the Casimir effect. J. Phys. Conf. Series **161**, 012001 (2009)
131. Pitaevskii, L.P.: Thermal Lifshitz Force between Atom and Conductor with Small Density of Carriers. Phys. Rev. Lett. **101**, 163202 (2008)
132. Grynberg, G., Robilliard, C.: Cold atoms in dissipative optical lattices. Phys. Rep. **355**, 335 (2001)
133. Bloch, I., Dalibard, J., Zwerger, W.: Many-body physics with ultracold gases. Rev. Mod. Phys. **80**, 885 (2008)
134. Derevianko, A., Obreshkov, B., Dzuba, V.A.: Mapping Out Atom-Wall Interaction with Atomic Clocks. Phys. Rev. Lett. **103**, 133201 (2009)
135. Moreno, G.A., Dalvit, D.A.R., Calzetta, E.: Bragg spectroscopy for measuring Casimir–Polder interactions with Bose–Einstein condensates above corrugated surfaces. New J. Phys. **12**, 033009 (2010)